THE GEOLOGICAL SOCIETY OF AMERICA®

Deep-water channel morphologies, architectures, and population densities in relation to stacking trajectories and climate states

Chenglin Gong[1,2,†], Ronald J. Steel[3], Kun Qi[1,2], and Yingmin Wang[1,2]
[1]*State Key Laboratory of Petroleum Resources and Prospecting, China University of Petroleum (Beijing), Beijing 102249, China*
[2]*College of Geosciences, China University of Petroleum (Beijing), Beijing 102249, China*
[3]*Department of Geological Sciences, Jackson School of Geosciences, University of Texas, Austin, Texas 78712, USA*

ABSTRACT

Deep-water channel morphologies, stratigraphy, and population densities in relation to stacking trajectories and climate states remain poorly constrained, and are highlighted by a sampling of 142 submarine channels. From the perspective of channel kinematics, turbidite channels exhibit tripartite lateral - random - vertical trajectories or unidirectional channel-complex trajectories, whereas contourite channels display oblique upslope trajectories. Turbidite channels tend to be deep and narrow and have two to three times more lateral migration than contourite channels, whereas contourite channels tend to be shallow and wide and have two to three times more vertical accretion. We relate such differences between channel morphology and stratigraphy to density contrast between flow and ambient fluid for contourite versus turbidite channels, which seems to have favored lateral channel migration in turbidite channels but channel thalweg deposition in contourite channels. Additionally, channels formed during a greenhouse climate state display low degrees of morphological and architectural variations, and are the minority in our global channel database (8% of total), although the Earth has been in a greenhouse state for 72% of the past 540 m.y. Icehouse channels, in contrast, exhibit high amplitudes of morphological and architectural variations and are the majority in the global channel family (92% of total), although the Earth has been in an icehouse state for 18% of the past 540 m.y. Such differences in channel-population densities between greenhouse and icehouse climates (8% versus 92%) suggest a weak global correlation of channel-population densities with warming greenhouse climates.

INTRODUCTION

Submarine channels or canyons have been the focus of extensive research since their discovery in the early 20th century (e.g., Daly, 1936; Shepard and Emery, 1941; Wynn et al., 2007; Peakall and Sumner, 2015; Fildani, 2017; Symons et al., 2017). This is largely because they: (1) are the fundamental building blocks of deep-water systems (e.g., Peakall and Sumner, 2015) and play a significant role in shaping and building continental margins (e.g., Peakall and Sumner, 2015); (2) can be seen to traverse hundreds of kilometers on the modern seafloor (e.g., Peakall and Sumner, 2015); (3) serve as the major conduits for the delivery of vast amounts of sediments, nutrients, pollutants, and carbon to deep-water areas (Galy et al., 2007; Talling et al., 2007; Hubbard et al., 2014; Fildani, 2017); (4) preserve critical signals of paleoclimatic and paleoceanographic information from their source regions (Hohbein and Cartwright, 2006; Gong et al., 2013) and are, thus, a key record of global change (Peakall et al., 2000); and (5) can form major subsurface oil and gas reservoirs in locations worldwide (Mayall et al., 2006; Janocko et al., 2013).

Based on the interpreted flow processes involved in their formation and construction, deep-water channels can be broadly grouped into two categories, namely turbidite channels created solely by downslope turbidity currents (e.g., Sumner et al., 2014; Symons et al., 2017) and contourite channels constructed mainly by along-slope contour currents (e.g., Rebesco et al., 2014). Turbidite channels are typically oriented parallel or subparallel to the depositional dip of the regional slope (i.e., roughly perpendicular to isobaths) and laterally migrate in an unsystematic manner (e.g., Wynn et al., 2007; McHargue et al., 2011; Peakall and Sumner, 2015), whereas contourite channels are generally oriented parallel or subparallel to the depositional strike of the regional slope (i.e., roughly parallel to isobaths) and consistently migrate in an oblique upslope direction (Rebesco et al., 2014; Gong et al., 2017). In addition to these two types of channels created mainly by turbidity or contour currents, an alternative type of submarine channels (i.e., unidirectionally migrating deep-water channels, *sensu* Gong et al. [2013]) created by the combined action and interplay of turbidity and contour currents was recently recognized in the Pearl River Mouth Basin (northern South China Sea; Gong et al., 2013), the Lower Congo Basin (Gong et al., 2018), the Tanzania Coastal Basin (Sansom, 2018), offshore northern Mozambique (Fonnesu et al., 2020), and the Nova Scotia margin (offshore southeastern Canada; Campbell and Mosher, 2016; Miramontes et al., 2020). They are oriented subparallel to the depositional dip of the regional slope (i.e., indicative of turbidity flows) but have consistently migrated parallel or subparallel to isobaths (i.e., suggestive of contour currents) (Gong et al., 2013, 2018; Campbell and Mosher, 2016; Sansom, 2018; Fonnesu et al., 2020; Miramontes et al., 2020).

Despite many years of study, the characterization of channel stratigraphy and architectures has been proven to be challenging (e.g., McHargue et al., 2011; Janocko et al., 2013; Jobe et al., 2015). Adapting trajectory analysis for deep-water channels (i.e., systematic channel-growth trajectories or pathways in any stratigraphic succession) (e.g., Sylvester et al., 2011; Sylvester and Covault, 2016; Jobe et al., 2016) may boost our ability to characterize channel architectures and stratigraphy, as highlighted by Labourdette and Bez (2009), McHargue et al. (2011), and Jobe et al. (2016). Channel kinematics or trajectory analysis is, therefore, considered a recent advancement in the characterization of channel stratigraphy and architectures (e.g., Sylvester et al., 2011; Jobe et al., 2016). Previous studies of channel-growth trajectories, however, have mainly focused on well-documented turbidite channels (e.g., Sylvester et al., 2011; Sylvester and Covault, 2016; Jobe et al., 2016) without much attention paid to contourite or unidirectionally migrating deep-water channels.

[†]chenglingong@cup.edu.cn.

GSA Bulletin; January/February 2021; v. 133; no. 1/2; p. 287–306; https://doi.org/10.1130/B35431.1; 17 figures; 1 supplemental file.
published online 15 June 2020

In addition, an increasing number of studies have suggested that climatic perturbations play an important role in the modulation of flow dynamics and stratigraphy of submarine channels (e.g., Henrich et al., 2010; Zhang et al., 2018; Sequeiros et al., 2019). For example, previous studies have highlighted the potential effects of storms (Puig et al., 2004), El Niño–Southern Oscillation (Covault et al., 2010), Indo-Asian monsoon (Fournier et al., 2016), and major typhoons (e.g., Zhang et al., 2018; Sequeiros et al., 2019) on the timing, intensity, and frequency of submarine channel turbidity currents. However, it remains an open question as to how deep-time channel stratigraphy has responded to two end-member climatic conditions (i.e., icehouse and greenhouse climates) (e.g., Hodgson et al., 2018; Sømme et al., 2019).

There are, therefore, at least two further challenges in deep-water channel stratigraphy research. First, how is channel morphology and architecture impacted by temporal changes in channel trajectory? Second, does channel stratigraphy respond to changes in deep-time climates (i.e., icehouse and greenhouse)? A global channel database of 142 deep-water channels (Tables S1–S3 in the Supplemental Material[1]; Fig. 1A) is established to investigate these two research questions.

DEEP-WATER CHANNEL TERMINOLOGY SYSTEM

Industry and academic practitioners have investigated channels in various deep-water basins worldwide, leading to a proliferation of nomenclature, such as geobodies, channel elements, channel belts, etc. (e.g., Mayall et al., 2006; Wynn et al., 2007; Gong et al., 2013). A terminology system (story → channel fill → channel complex → channel-complex set → submarine channel, as graphically illustrated in Fig. 2) is adopted herein to delineate different hierarchies of deep-water channels. In this channel-terminology system, *story* is the lowest level and smallest depositional element of the stratigraphic hierarchy, and refers to a volume of sediments bounded by local erosional scours (Fig. 2). The clustering of stories into a story set is termed *channel fill* (Fig. 2) (Edwards et al., 2017). The volume of sediments deposited during a single cycle of multiple channel-filling periods before abandonment is called a *channel complex* (*sensu* Sprague et al., 2002), which, therefore, represents a coherent package of channel-related deposits (Fig. 2). Two or more genetically related channel complexes of similar architectural style is called a *channel-complex set* (Fig. 2). Through time, different channel-complex sets laterally migrate and vertically stack upon one another, resulting in a given deep-water channel that records a single cycle of channel cutting, filling, avulsion, and abandonment (Fig. 2).

Morphological and architectural parameters as well as other indices of submarine channels as documented in this study are: (1) *channel width* (*W*)—measured as the maximum horizontal distance between channel banks (i.e., levee crests) (Fig. 2) (see also Janocko et al., 2013); (2) *channel thickness* (*T*)—measured as the maximum vertical relief from the channel base in the axial zone to the channel banks (Fig. 2); (3) *aspect ratio* (*W*/*T*)—channel width divided by channel thickness; (4) *trajectory angle* (T_c)—defined in the Methodology section (Fig. 2); and (5) *channel mobility number* (M_s)—defined as the ratio of avulsion and lateral-migration time scales (Jobe et al., 2016; see the methodology section for full details).

GLOBAL DEEP-TIME CHANNEL DATABASE AND METHODOLOGY

Global Deep-Time Channel Database

A global channel database of 142 deep-water channels of different origins, all of which are from siliciclastic margins, has been established (see Tables S1–S3 [footnote 1] for full details; Fig. 1A). Fifty (50) channel examples indicated by numbered red circles in Figure 1A are commonly oriented parallel or subparallel to the direction of downslope flow (Table S1 [footnote 1]), suggesting that turbidity currents were the principal processes operating within them (i.e., turbidite channels). In contrast, 49 channel examples indicated by numbered white circles in Figure 1A are parallel or subparallel to the direction of along-slope flow (Table S2 [footnote 1]), indicating that contour currents were mainly responsible for their construction (i.e., contour channels). Forty-three (43) channel examples indicated by numbered blue circles in Figure 1A are commonly oriented parallel or subparallel to the direction of downslope gravity flows, but consistently migrated parallel or subparallel to isobaths, suggesting that both turbidity and contour currents were collectively involved in their construction (i.e., unidirectionally migrating deep-water channels). The data sources used in this study include both published and unpublished seismic data, on which seismically well-imaged deep-water channels at deep-time scale are seen (Tables S1–S3 [footnote 1]).

Methodology

The current research makes use of the concept of *channel-complex trajectory*, which is analogous to shoreline or shelf-edge trajectory, and is adapted here as a descriptor for the successive or sequential lateral and vertical movements of individual channel complexes that do not contain significant erosion (Fig. 2). A specific channel-complex trajectory records the migration of two or more genetically related channel complexes (i.e., a channel-complex set), and is represented by trajectory angles (T_c), computed by:

$$T_c = \arctan\left(dy / dx\right), \quad (1)$$

where *dx* and *dy* are, respectively, lateral and vertical components of a specific channel-growth trajectory (Fig. 2). We refer positive values of *dx* to the lateral channel migration parallel to the depositional strike of the regional slope, but negative values of *dx* to the lateral channel migration parallel to the depositional dip of the regional slope (i.e., an oblique upslope migration) (Fig. 2).

In addition, other properties and parameters of the studied deep-water channels have been statistically analyzed in terms of channel width (*W*), channel thickness (*T*), aspect ratio (*W*/*T*), channel-population density, and channel mobility number (M_s). *Channel-population density* refers to the mass of a given type of submarine channels divided by the overall volume of the chosen channel examples (i.e., 142). For example, among the 142 chosen channel examples, 12 channel examples are grouped into submarine greenhouse channels, resulting in a channel-population density of 12/142 = 8% for submarine greenhouse channels (Fig. 1C). Moreover, channel mobility number (M_s) is computed by (Jerolmack and Mohrig, 2007):

$$M_s = \frac{|dx|}{dy}\frac{T}{W}. \quad (2)$$

Our measurements of channel-complex kinematics (*dx* and *dy*) and channel morphometrics (*T* and *W*) are not decompacted, and generally agree with some of our measurements from modern topographic data (Tables S1–S3 [footnote 1]), suggesting that the decompaction of the channel form would not significantly alter the results of our calculation of T_c, *W*/*T*, and M_s (see also Jobe et al., 2016).

CLASSIFICATION AND QUANTIFICATION OF 142 DEEP-WATER CHANNELS BASED ON TRAJECTORY REGIME

The 142 reviewed deep-water channels exhibit five main trajectory classes, namely

[1]Supplemental Material. Morphometrics and architectures of 142 chosen deep-water channels and their relation to stacking trajectories and climates. Please visit https://doi.org/10.1130/12250025 to access the supplemental material, and contact editing@geosociety.org with any questions.

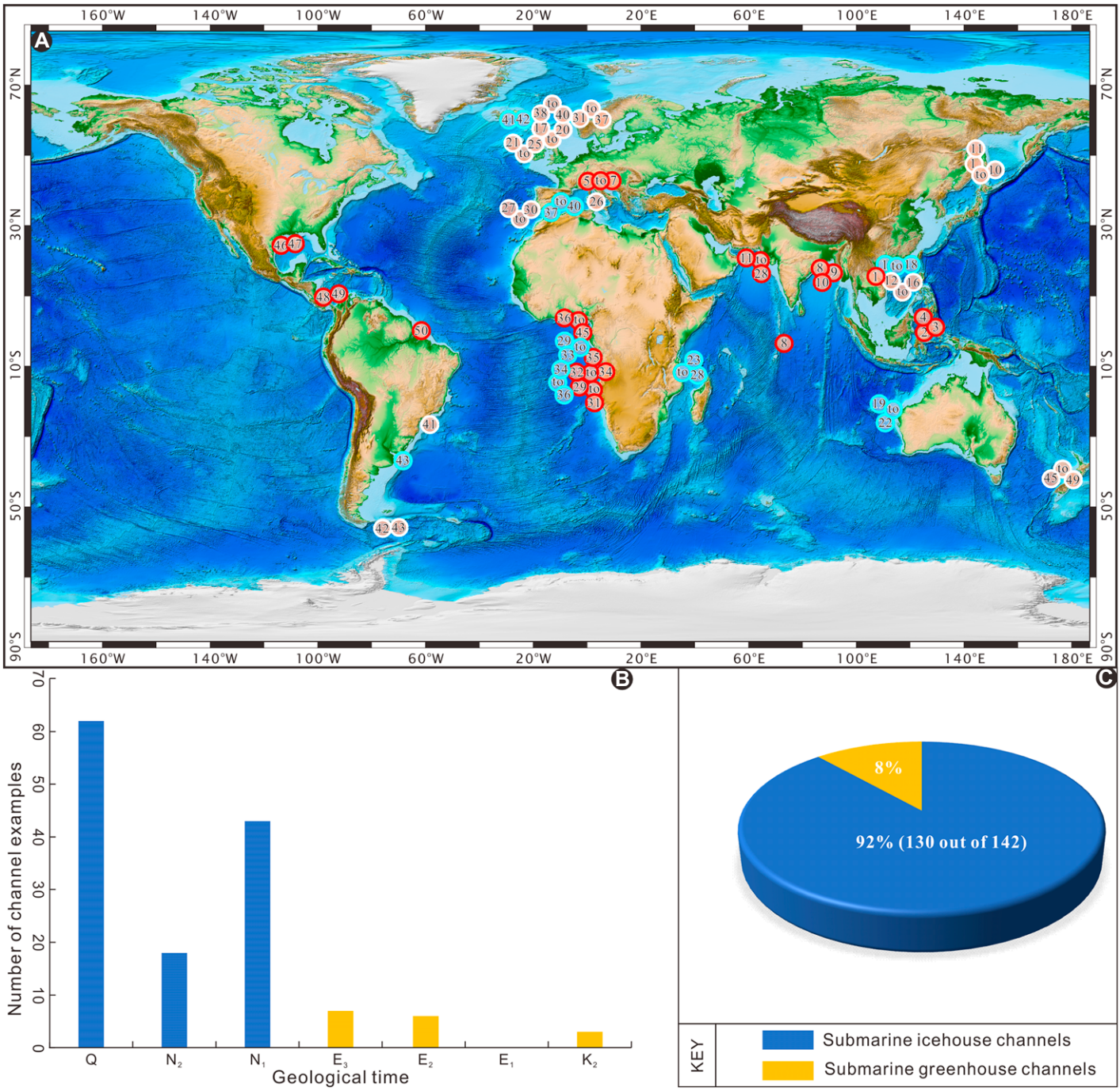

Figure 1. (A) Global bathymetric map showing locations of the studied turbidite, contourite, and unidirectionally migrating channels (indicated by red, white, and blue numbered circles, respectively). The base map (ETOPO1) presented in this figure was obtained from the U.S National Geophysical Data Center website (http://www.ngdc.noaa.gov/mgg/global/global.html); image authors are J. Varner and E. Lim, University of Colorado at Boulder. (B) Histogram illustrating the occurrence of channel examples, plotted as the geologic time of deposition (K_2—Late Cretaceous; E_1—Paleocene; E_2—Eocene; E_3—Oligocene; N_1—Miocene; N_2—Pliocene; Q—Quaternary). (C) Pie diagram showing channel-population densities of submarine greenhouse versus icehouse channels.

lateral, random, vertical, oblique upslope, and unidirectional trajectories (Tables S1–S3 [footnote 1]; Fig. 3). The trajectory concept is used below for deciphering the stacking migration of channel complexes.

Lateral Channel-Complex Trajectories

The first population of channel-complex trajectories contains channel complexes that have migrated in a dominantly lateral direction, thereby displaying a growth trajectory referred to herein as a *lateral channel-complex trajectory* (Fig. 3A). Representative examples of channel-complex sets with lateral channel-complex trajectories are shown by blue dots in Figures 4

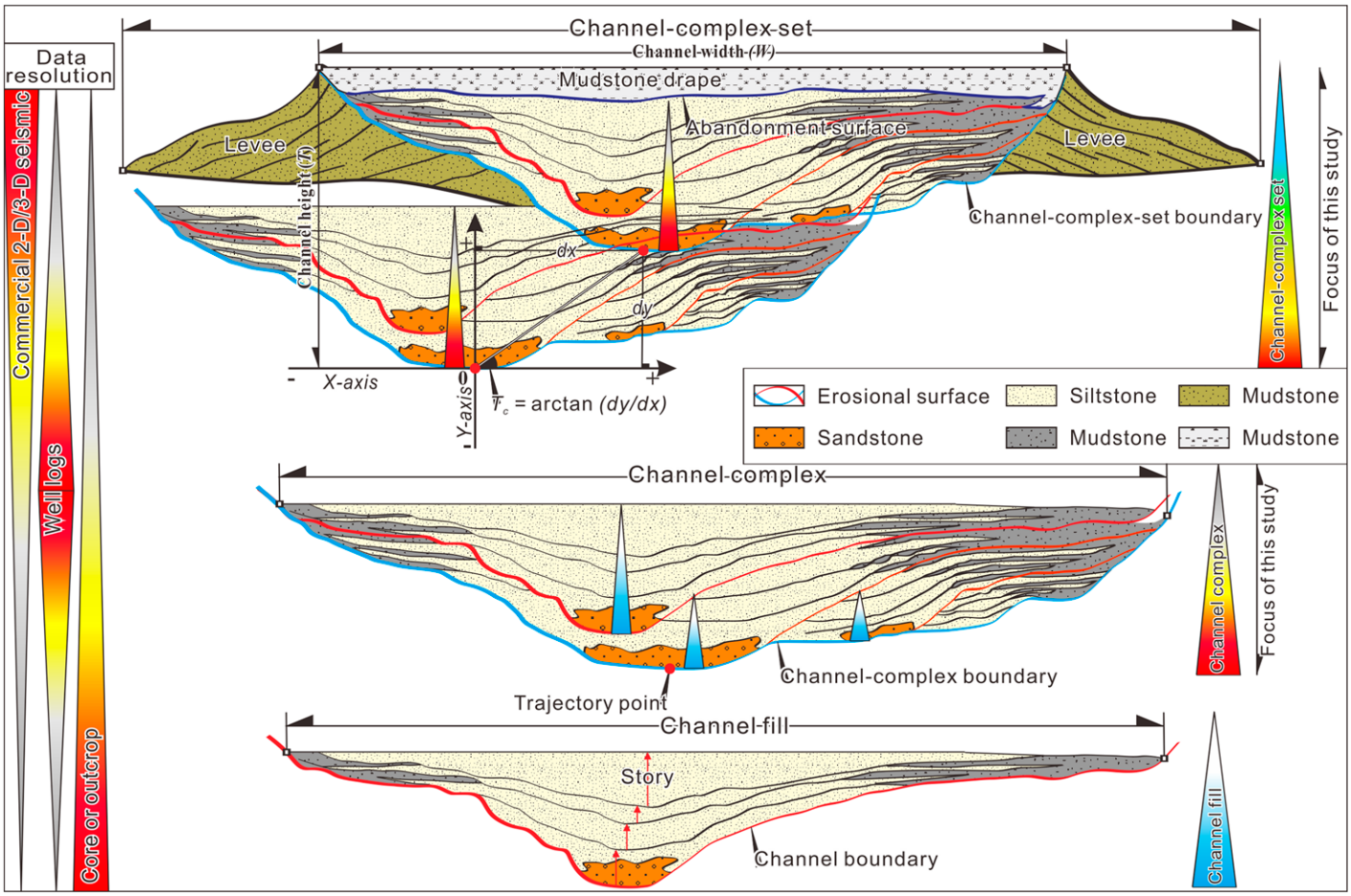

Figure 2. Schematic illustration of the hierarchical framework of deep-water channels and the methodology used to determine channel-complex trajectories and morphologies. The shown channel hierarchical framework was compiled from Sprague et al. (2002) and Edwards et al. (2017). 2-D, 3-D—two-, three-dimensional; T_c—trajectory angle.

and 5, and channel complexes with such trajectories are generally seen to occur within the lower fill level of a large-scale turbidite channel. Lateral channel-complex trajectories have relatively low T_c of 1.4° to 4.1°, with a mean value of 2.4° and a standard deviation of ±0.9° (Table S1 [footnote 1]; Fig. 6A).

Morphologically, turbidite channel-complex sets with lateral channel-complex trajectories exhibit tortuous channel courses (Figs. 3A′ and 5A). They have *W* of 404–3992 m (averaging 2313 m) and *T* of 26–196 m (averaging 102 m), giving rise to a moderate *W*/*T* of 11–42, with a mean value of 24 and a standard deviation of ±10 (Table S1 [footnote 1]; Figs. 6A and 7A). Architecturally, turbidite channels with lateral channel-complex trajectories are characterized by large values of M_s ranging from 0.76 to 1.89 (averaging 1.21), with a standard deviation of ±0.32 (Fig. 8A), and have migrated in a direction parallel or subparallel to the isobaths, collectively pointing to organized lateral channel stacking patterns (Figs. 3A, 4, and 5A).

Random Channel-Complex Trajectories

The second population of channel-complex trajectories comprises individual channel complexes that have randomly migrated in both lateral and vertical steps, displaying a trajectory trend referred to herein as a *random channel-complex trajectory* (Figs. 3B, 4 and 5). Representative examples of channel-complex sets with random channel-complex trajectories are shown by yellow dots in Figures 4 and 5. Channel complexes with such trajectories are commonly confined within the middle fill level of a larger-scale turbidite channel (e.g., Figs. 4 and 5). Random channel-complex trajectories have variable T_c ranging from 1.8° to 5.9°, with a mean value of 3.3° and a standard deviation of ±1.4° (Table S1 [footnote 1]; Fig. 6A).

Morphologically, turbidite channel-complex sets with random channel-complex trajectories are flanked by inner levees (e.g., Figs. 4A and 4B), and are commonly characterized by smoothly curved meander bends (Fig. 3B′). They have *W* of 825–3589 m (averaging 2270 m) and *T* of 72–187 m (averaging 123 m), resulting in moderate *W*/*T* of 10–24, with a mean value of 18 and a standard deviation of ±5 (Table S1 [footnote 1]; Figs. 6A and 7A). Architecturally, turbidite channels with random channel-complex trajectories display M_s ranging from 0.60 to 1.81 (averaging 1.17) (Figs. 8A), and laterally migrated and vertically nested in a disorganized manner, resulting in disorganized stacking patterns (Figs. 3B, 4, and 5A).

Vertical Channel-Complex Trajectories

The third population of channel-complex trajectories consists of a series of channel complexes that are strongly aggradational and have accreted in a dominantly vertical direction through time, thus showing a trajectory tendency referred herein to as a *vertical channel-complex trajectory* (Figs. 3C, 4, 5B, and 9). Representative examples with vertical channel-complex trajectories are shown by red

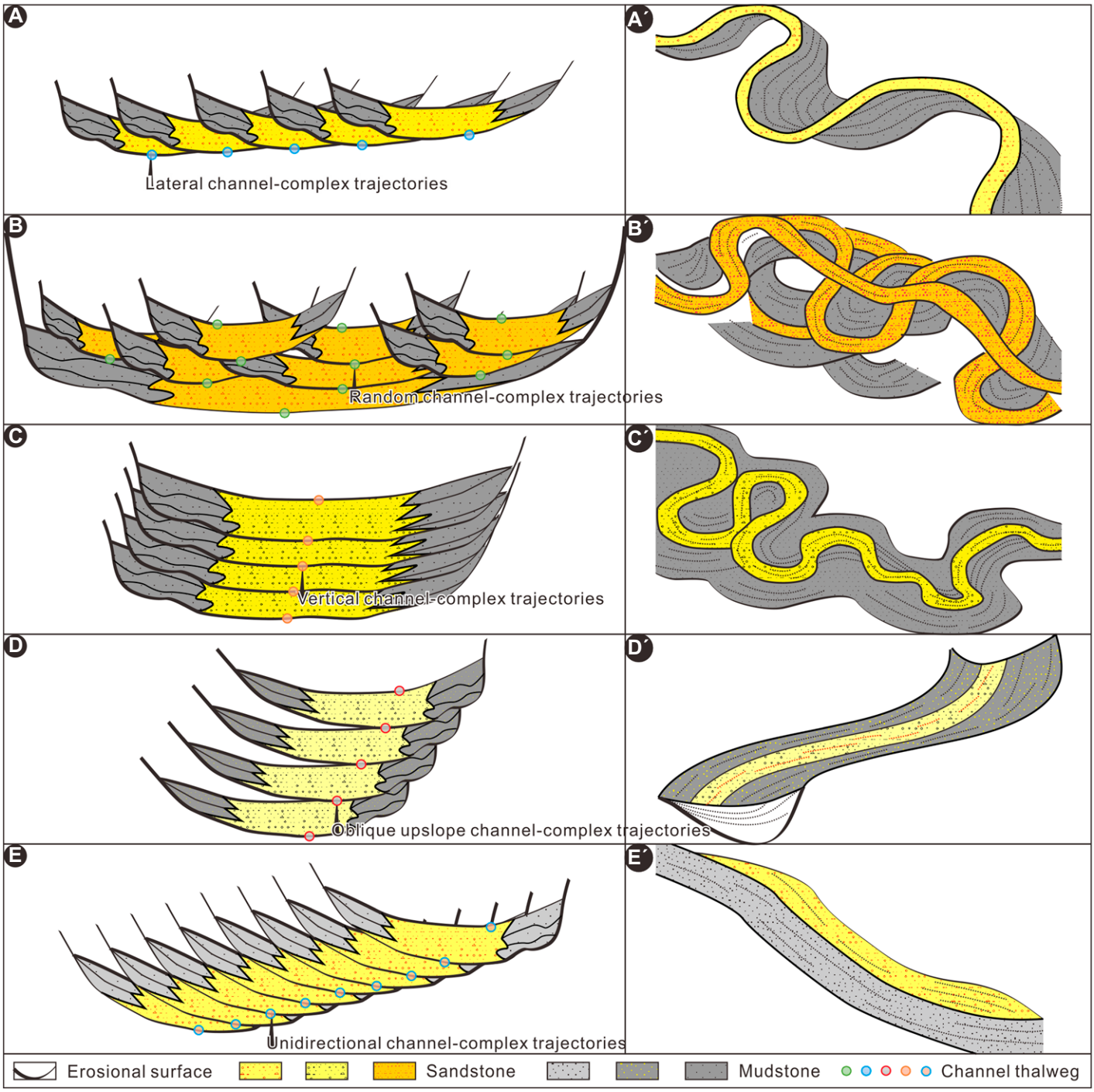

Figure 3. Schematic illustrations of section (left panels) and plan (right panels) views of channel-complex sets with different channel-complex trajectory regimes.

dots in Figures 4, 5B, and 9. Channel complexes with such trajectories are commonly seen to be confined within the upper fill level of a larger-scale turbidite channel (Figs. 4 and 5B). They exhibit relatively high T_c of 12.0° to 59.0°, with a mean value of 29.9°and a standard deviation of ±14.9° (Table S1 [footnote 1]; Fig. 6A).

Morphologically, turbidite channel-complex sets with vertical trajectories are flanked by outer levees (see Figs. 4A, 4B, and 9 for some representative examples), and have tortuous and long fairways (Figs. 3C′ and 4B). They have *W* of 399–1970 m (averaging 950 m) and *T* of 85–299 m (averaging 191 m), resulting in low *W*/*T* of 2–9, with a mean value of 5 and a standard deviation of ±2 (Table S1 [footnote 1]; Figs. 6A and 7A). Architecturally, turbidite channels with vertical channel-complex trajectories have medium values of M_s ranging from 0.11 to 0.86 (averaging 0.44), with a standard deviation of ±0.22 (Fig. 8A), and have accreted in a dominantly vertical direction through time (e.g., Figs. 3C, 4, 5B, and 9). Their central parts

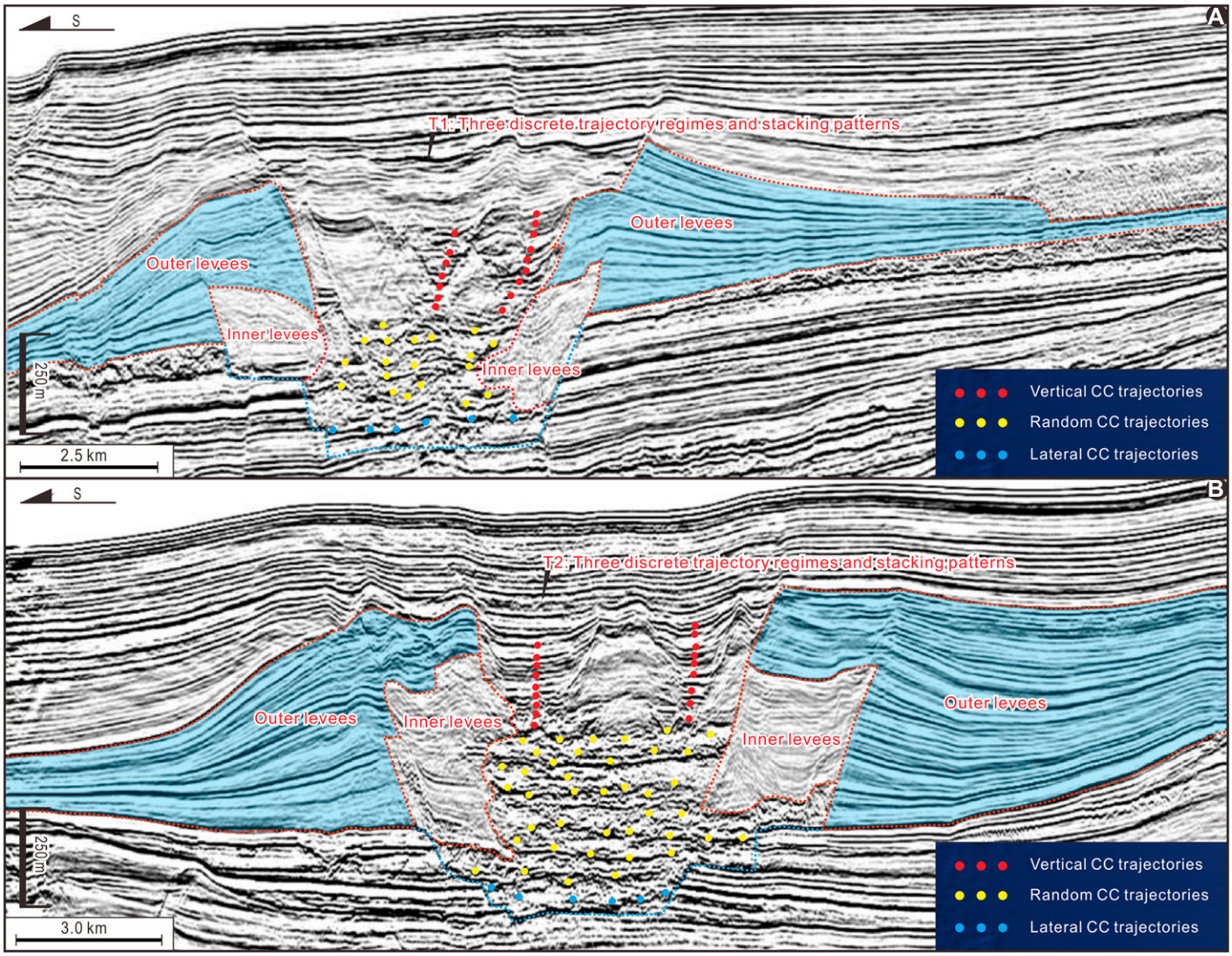

Figure 4. Indus Fan (Arabian Sea) seismic examples (from Deptuck et al., 2003) of turbidite channels exhibiting tripartite lateral - random - vertical channel trajectories (indicated by blue, yellow, and red dots, respectively). Note that channel complexes with random and vertical trajectories are, respectively, flanked by the inner and outer levees, but that those with lateral channel-complex (CC) trajectories are not.

are seismically imaged as narrow, highly sinuous high-amplitude bands (Fig. 9A), and appear on seismic section as dike-like high-amplitude, discontinuous reflection packages, organized overall as a vertical stacking pattern (Figs. 3C, 4B, 5B, and 9).

Oblique Upslope Channel-Complex Trajectories

The fourth population of channel-complex kinematics is composed of channel complexes that consistently migrated in an oblique upslope direction, thus exhibiting a trajectory trend referred herein to as an *oblique upslope channel-complex trajectory* (Figs. 3D, 10, and 11). Representative channel-complex sets with oblique upslope trajectories are indicated by blue dots in Figures 10 and 11E. Channel complexes with such trajectories represent the typical trajectory regime of contourite channels, and have negative values of T_c ranging from –89.8° to –40.2°, with a mean value of –74.1° and a standard deviation of ±15.1° (Table S2 [footnote 1]; Figs. 3D, 6B, and 8B).

Morphologically, 49 contourite channels with oblique upslope channel-complex trajectories contain upslope walls that are, overall, steeper than their downslope counterparts (e.g., Figs. 3D, 10, and 11E), and exhibit isobath-parallel channel courses (Figs. 3D′, 11A–11D). Morphologically, they have W of 430–4778 m (averaging 2148 m) and T of 21–178 m (averaging 60 m), giving rise to high W/T of 14–67, with a mean value of 39 and a standard deviation of ±17 (Table S2 [footnote 1]; Figs. 6B and 7B). Architecturally, stacked contourite channel-complex sets with oblique upslope trajectories consistently migrated in an oblique upslope direction, and exhibit low values of M_s ranging from 0.02 to 1.20 (averaging 0.28), with a standard deviation of ±0.29, thereby exhibiting oblique upslope offset stacking patterns (Figs. 3D and 8B).

Unidirectional Channel-Complex Trajectories

The fifth population of channel-complex trajectories consists of channel complexes that consistently migrated parallel or subparallel to isobaths through time, thereby creating

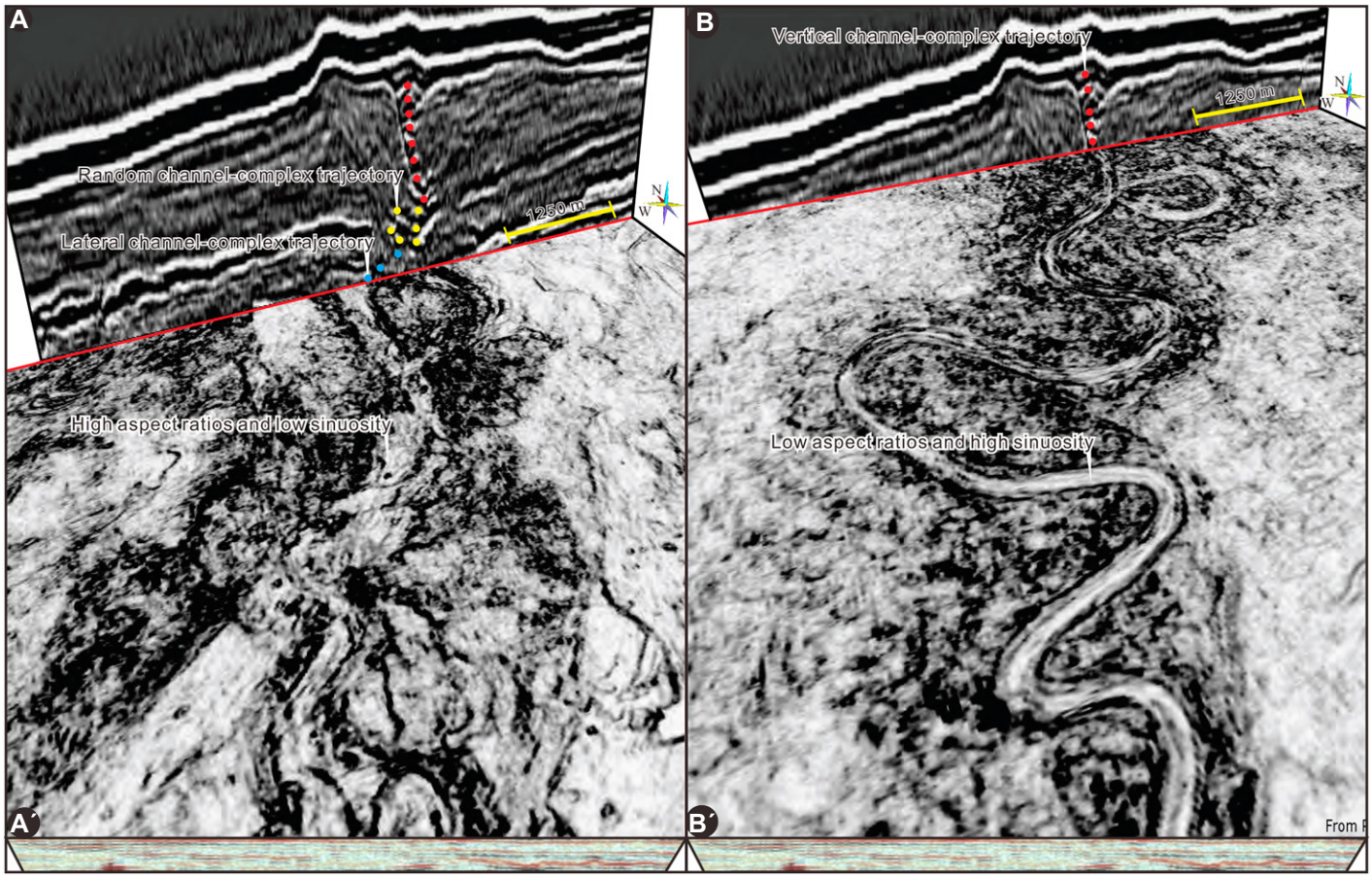

Figure 5. Comparison in channel stratigraphy and kinematics between channel complexes with lateral and random trajectories (A and A′) versus those with vertical trajectories (B and B′), based on seismic examples of turbidite channels from the Gulf of Mexico (from Posamentier, 2003). Tops (A and B) and bottoms (A′ and B′) of panels are cross-section and plan views of turbidite channels with tripartite lateral - random - vertical trajectories.

a *unidirectional channel-complex trajectory* (Figs. 3E, 12–14). Representative channel examples of this type are illustrated by arrowed lines in Figures 12–13 and by red dots in Figure 14. Channel complexes with such trajectories represent typical kinematics of unidirectionally migrating deep-water channels (e.g., Figs. 12–14). Representative seismic examples of channels with unidirectional channel-complex trajectories are from the Pearl River Mouth Basin of the northern South China Sea (Fig. 12A), the Lower Congo Basin (Fig. 12B), the Qiongdongnan Basin of the northeastern South China Sea margin (Figs. 13A and 13B), the southeastern Greenland margin (Figs. 14A and 14B), and the southeastern Brazilian margin (Fig. 14C; see Table S2 [footnote 1] for more examples). Channels with unidirectional trajectories have T_c of 5.1° to 44.4°, with a mean value of 13.8° and a standard deviation of ±10.7° (Table S3 [footnote 1]; Fig. 6A).

Morphologically, 43 studied examples of unidirectionally migrating deep-water channels collectively display asymmetrical cross-sections with steep channel walls toward the channel migration (Figs. 3E and 12–14). They have W of 434–4571 (averaging 1940 m) and T of 24–251 m (averaging 104 m), resulting in moderate W/T of 8–43, with a mean value of 20 and a standard deviation of ±8 (Table S3 [footnote 1]; Figs. 6A and 7A). Architecturally, submarine channels with unidirectional channel-complex trajectories have small values of M_s ranging from 0.06 to 0.79, with a mean value of 0.31 and a standard deviation of ±0.17 (Fig. 8A), and unidirectionally migrated and accreted through time, thereby displaying unidirectional offset stacking patterns (Figs. 3E and 12–14).

CLASSIFICATION AND QUANTIFICATION OF 142 DEEP-WATER CHANNELS FROM THE PERSPECTIVE OF CLIMATE STATES

Throughout the Earth's history, our planet's climate has been fluctuating between two main end-member climate states (i.e., icehouse and greenhouse times) (Blum and Hattier-Womack, 2009; Sømme et al., 2009; Kidder and Worsley, 2012). From the perspective of deep-time paleoclimates, the 142 channel examples under consideration are, thus, grouped into two main categories as discussed below.

Channels Developed during Greenhouse Climate

The Earth has been in an icehouse state for ~18% of the past 540 m.y. and in a greenhouse state for ~72% of the last 540 m.y. (e.g., Kidder and Worsley, 2012). The Cretaceous, Paleocene, Eocene, and Oligocene are all considered as greenhouse periods (Fig. 1B) (Stoll and Schrag, 1996; Miller et al., 1991, 2003; Kidder and Worsley, 2012). Some classical examples of submarine greenhouse channels are early Eocene channels on the northern Mozambique margin (UC23 to UC28 in Table S3 [footnote 1]; see also Fonnesu et al., 2020), Oligocene

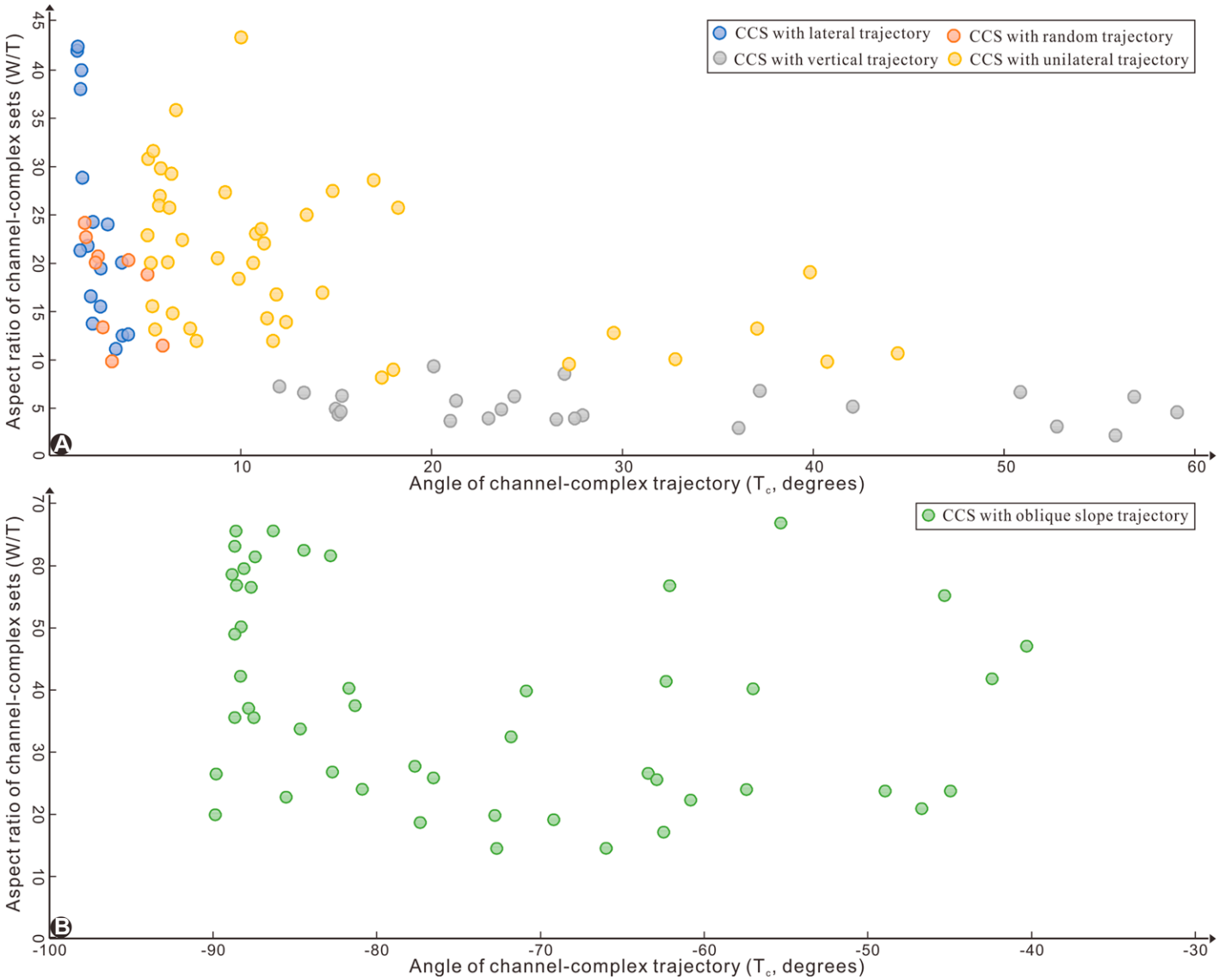

Figure 6. Cross-plots of channel-complex trajectories (represented by trajectory angle T_c) versus channel morphologies (proxied by the ratio of channel width to thickness, *W/T*) for 142 studied channels. CC—channel complex; CCS—channel-complex set.

channels on the Gabon slope (UC34 to UC36 in Table S3 [footnote 1]; see also Séranne and Abeigne, 1999), and contourite channels of Late Cretaceous age on the German North Sea margin (C39 to C40 in Table S2 [footnote 1]; see also Surlyk et al., 2008).

Among 142 chosen channel examples, only 12 reviewed channel cases are considered as submarine greenhouse channels, resulting in a low channel-population density of 12/142 = 8% (Figs. 1B and 1C). Submarine greenhouse channels are, therefore, the minority in the global channel community (Figs. 1B and 1C), although greenhouse climates have been the major paleoclimate states throughout the Earth's history (72%). These greenhouse channels have *W/T* ranging from 12 to 29 with a mean value of 17 and a standard deviation of ±5, and have M_s of 0.03–0.79 with a mean value of 0.36 and a standard deviation of ±0.27 (Tables S2 and S3 [footnote 1]; Figs. 15B).

Channels Developed during Icehouse Climates

The Miocene, Pliocene, and Quaternary are globally considered as icehouse periods (Fig. 1B) (Miller et al., 1991, 2003; Sømme et al., 2009), suggesting that considered deep-water channels (130 of 142) developed during Miocene, Pliocene, and Quaternary are therefore considered as icehouse channels (Table S1–S3 [footnote 1]; Fig. 1B). Submarine icehouse channels are, therefore, the majority in the global channel family (Figs. 1B and 1C), although icehouse climates are the minor paleoclimate states throughout the Earth's history (18%). Some classical examples of submarine icehouse channels are from the Pliocene Bengal Fan (Bay of Bengal; Fig. 9), Miocene Santos Basin (southwestern Atlantic Ocean; Fig. 11), Miocene to Quaternary Pearl River slope (Fig. 12A), Pliocene Qiongdongnan margin (Fig. 13), as well as some seismically well-imaged examples of Quaternary icehouse channels seen in Figures 4, 5, 10, 13, and 14.

The 130 reviewed submarine channels considered as icehouse channels (see Tables S1–S3 [footnote 1] for full details) result in a high channel-population density of 130/142 = 92% (Figs. 1B and 1C). These submarine icehouse

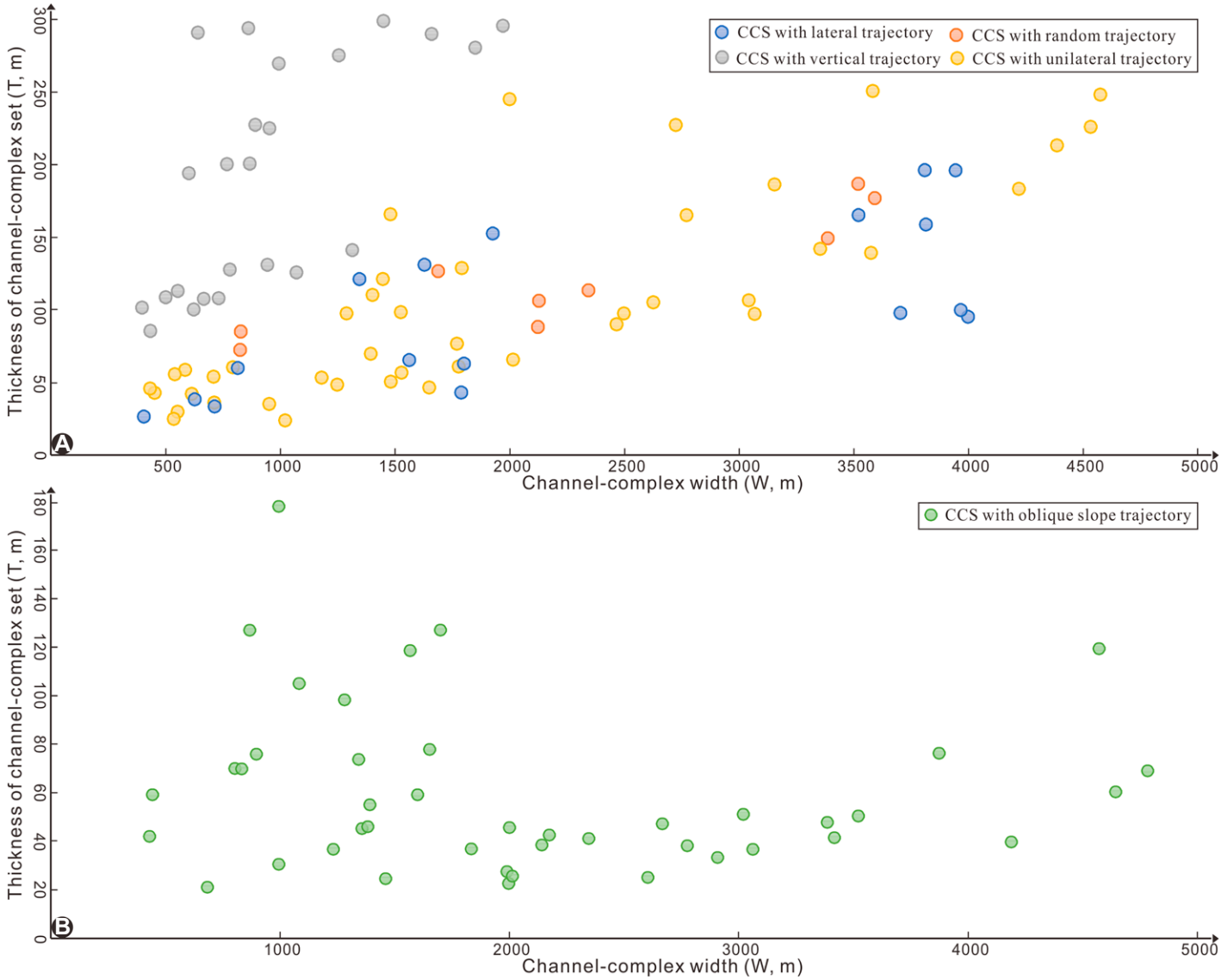

Figure 7. Cross-plots of channel width (*W*) versus thickness (*T*) for turbidite (A) and contourite (B) channel-complex sets. CC—channel complex; CCS—channel-complex set.

channels have *W/T* ranging from 2 to 67, with a mean of 25 and a standard deviation of ±17. They are also characterized by a wide range of M_s varying from 0.02 to 1.89 with a mean value of 0.50 and a standard deviation of ±0.44 (Tables S1–S3 [footnote 1]; Fig. 15B).

TURBIDITE AND CONTOURITE SUBMARINE CHANNELS GROUPED ACCORDING TO STACKING PATTERN AND CLIMATE STATE

From the perspective of channel stacking patterns, 142 studied channels can be grouped into turbidite channels with tripartite lateral - random - vertical or unidirectional channel-complex trajectories, and contourite channels with oblique upslope channel-complex trajectories. From the perspective of climate states, they can be grouped into submarine greenhouse and icehouse channels. In this section, we explore the difference in channel morphology and architecture for turbidite versus contourite channels and for greenhouse versus icehouse channels.

Comparison of Channel Morphologies and Architectures between Different Trajectory Regimes

Regarding channel morphology, the 93 examples of turbidite channels with tripartite lateral - random - vertical or unidirectional channel-complex trajectories have relatively low *W/T* ranging from 2 to 43, with a low mean value of 17, a low median value of 15, and a low standard deviation of ±10 (Figs. 15A and 16A). The 49 examples of contourite channels with oblique upslope channel-complex trajectories, in contrast, have relatively high *W/T* ranging from 14 to 67, with a high mean value of 39, a high median value of 37, and a high standard deviation of ±17 (Figs. 15A and 16A). Values of *W/T* for contourite channels are, thus, almost two to three times larger than those of turbidite channels (Fig. 16A). This, together with the fact that mean, median, and standard deviation values of *W/T* for contourite channels are almost two to three times higher than those of turbidite channels (Fig. 16A), suggests that contourite channels tend to be shallow and wide, whereas

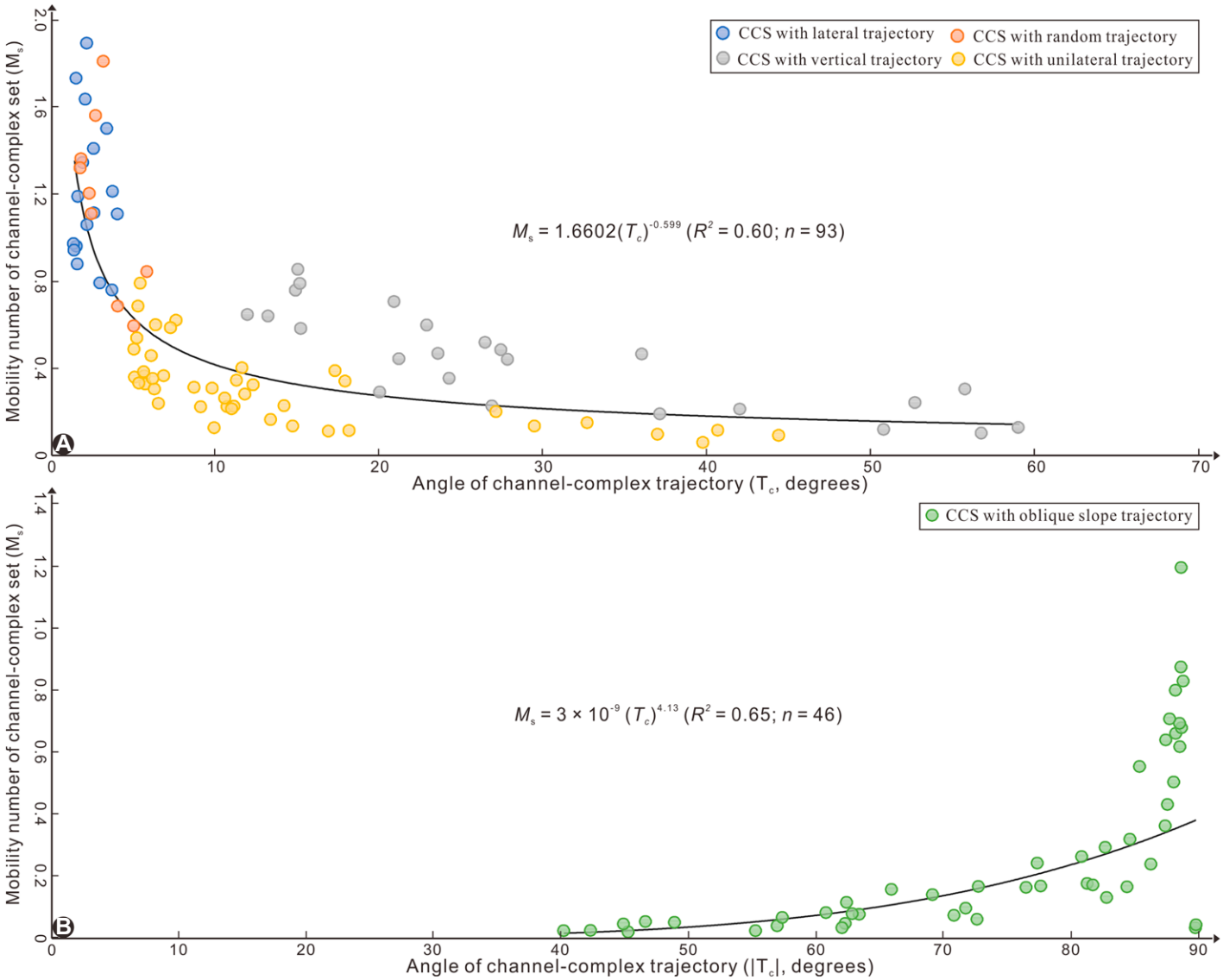

Figure 8. Cross-plots of trajectory angle (T_c) versus channel mobility number (M_s) for turbidite (A) and contourite (B) channel-complex sets. Note that T_c versus M_s follows a power-law relationship. CC—channel complex; CCS—channel-complex set.

turbidite channels tend to be deep and narrow (Figs. 15A and 16A).

As regards channel stacking and architectures, the 93 reviewed turbidite channels with tripartite lateral - random - vertical or unidirectional channel-complex trajectories are characterized by relatively high mobility with M_s ranging from 0.06 to 1.89, with a high mean value of 0.59, a high median value of 0.45, and a high standard deviation of ±0.45 (Figs. 15A and 16B). The 49 examples of contourite channels with oblique upslope channel-complex trajectories, in contrast, are characterized by relatively low mobility with M_s varying from 0.02 to 1.20, with a low mean value of 0.28, a low median value of 0.16, and a low standard deviation of ±0.29 (Figs. 15A and 16B). Turbidite channels, therefore, have a mobility (M_s) that is almost two to three times greater than that of contourite channels (Figs. 15A and 16B). Previous studies have suggested that low M_s values are symptomatic of abundant vertical channel aggradation but little lateral migration, whereas high M_s values are suggestive of abundant lateral channel migration but little aggradation (Sylvester et al., 2011; Jobe et al., 2016). This, together with the fact that mean, median, and standard deviation values of M_s for turbidite channels are also almost two to three times larger than those of contourite channels (Fig. 16A), suggests that turbidite channels have two to three times more lateral migration (with low aggradational potential), but that contourite channels have two to three times more tendency to vertically accrete.

Comparison in Channel Morphologies and Architectures between Different Climate States

As regards channel morphology, the 12 greenhouse channel examples have a narrow range of *W/T* (12–29), with a relatively low mean value of 17, a relatively low median value of 15, and a relatively low standard deviation of ±5 (Tables S1–S3 [footnote 1]; Figs. 15B and 17A). The 130 reviewed cases of icehouse channels, in contrast, have a relatively wide range of *W/T* (2–67), with a relatively high mean value of 25, a relatively high median value of 22, and a relatively high standard deviation of ±17 (Tables S1–S3 [footnote 1]; Figs. 15B and 17A). The mean, median, and standard

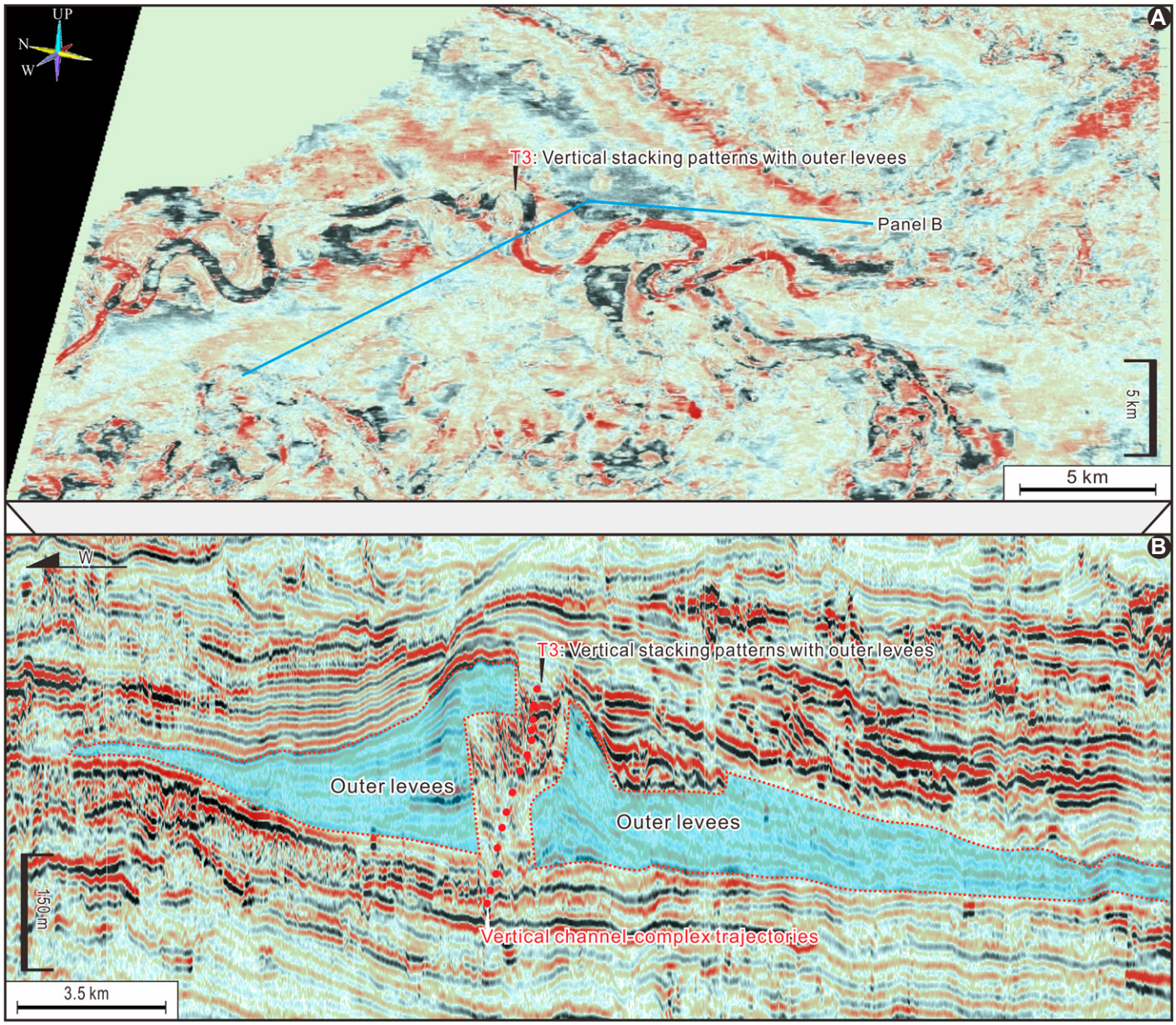

Figure 9. Unpublished seismic examples of turbidite channels with vertical channel-complex trajectories seen in plan-view amplitude slice (A) and seismic section (B). The shown channel example is flanked by volumetrically significant outer levees, and display vertical channel stacking patterns.

deviation of *W/T* for submarine icehouse channels are, thus, almost one to two times larger than those of submarine greenhouse channels (Fig. 17A). These observation suggest that icehouse channels display a significantly greater morphological variation than their greenhouse counterparts (Fig. 17A).

As regards channel stacking and architectures, the 12 reviewed deep-water greenhouse channels have a narrow mobility range with M_s ranging from 0.03 to 0.79, with a relatively low mean value of 0.36, a relatively high median value of 0.37, and a relatively low standard deviation of ±0.27 (Tables S2 and S3 [footnote 1]; Figs. 15B and 17B). The 130 reviewed deep-water icehouse channels, in contrast, have a relatively wide mobility range with M_s ranging from 0.02 to 1.89, with a relatively high mean value of 0.50, a relatively low median value of 0.35, and a relatively high standard deviation of ±0.44 (Tables S1–S3 [footnote 1]; Figs. 15B and 17B). The mean value and standard deviation of M_s for icehouse channels are, thus, almost one to two times larger than those of greenhouse channels (Fig. 17B). These observations suggest that icehouse channels display a significantly greater architectural variation than their greenhouse counterparts (Fig. 17B).

WHAT CONTROLS GLOBAL DIFFERENCES IN CHANNEL MORPHOLOGIES AND ARCHITECTURES?

Various mechanisms have been proposed to explain the differences in submarine channel morphology and architecture, including allogenic responses to unsteady forcing such

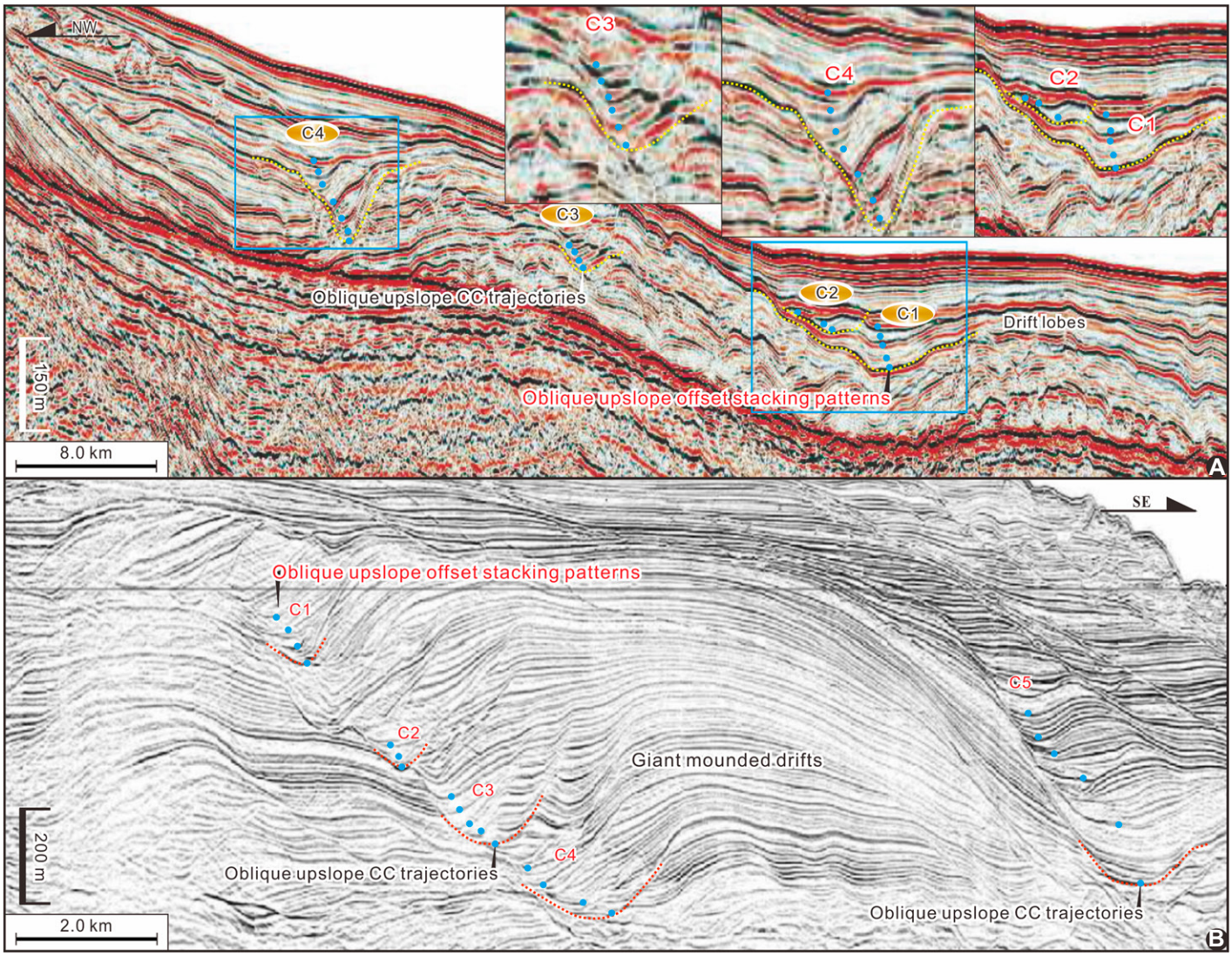

Figure 10. Dip-oriented seismic lines from the Faeroe-Shetland margin (A; from Davies et al., 2001) and offshore Canterbury Basin, New Zealand (B; from Lu et al., 2003), showing contourite examples (C1 to C4 on panel B and C1 to C5 on panel B) with oblique upslope channel-complex (CC) trajectories and oblique upslope offset stacking patterns.

as Coriolis forces or centrifugal forces (e.g., Kolla et al., 2007; Cossu et al., 2015; Peakall and Sumner, 2015) and autogenic responses to steady forcing such as the properties of turbidity currents (e.g., Kolla et al., 2007; Covault et al., 2016; Jobe et al., 2016). The channel data sets utilized in this study were collected from a wide range of sediment flux regimes, tectonic settings, ages, etc. We, therefore, limit our discussions only to the properties of flow processes that are present in the considered deep-water channels. As discussed earlier, contourite channels tend to be shallow and wide and have a fairly vertical style of channel stacking (represented by a low mean value of $M_s = 0.28$), whereas turbidite channels tend to be deep and narrow and have a laterally migrating style of channel stacking (Tables S1–S3 [footnote 1]; Figs. 15A, 16A, and 16B). Such contrast in channel morphology and architecture between turbidite and contourite channels may conceivably relate at times to the tectonic setting of the slope system, particularly to the subsidence rate of the slope. However, this hypothesis is beyond the scope of our research, because we lack the information on tectonic settings of individual slope-channel examples listed in Tables S1–S3 (footnote 1) (Fig. 1A). Instead, we suggest that the difference in the resultant morphology and stacking of contour-current and turbidity-current channels is more likely related to the density contrast (flow versus ambient fluid).

Turbidity currents carry a significant sedimentary load and are episodic, local, and intense (Azpiroz-Zabala et al., 2017), whereas contour currents are consist of essentially clean water and are long lived (up to millions of years) (Rebesco et al., 2014; Gong et al., 2018). Turbidity currents operating within turbidite channels, therefore, would have a greater density contrast with the ambient fluid than contour currents in contourite channels. The high density difference between turbidity currents and ambient fluid would decrease the potential for overspill and flow stripping. This, in turn, would favor channel thalweg deposition (Pirmez and Imran, 2003; Jobe et al., 2016), resulting in more lateral migration (represented by a higher mean value of

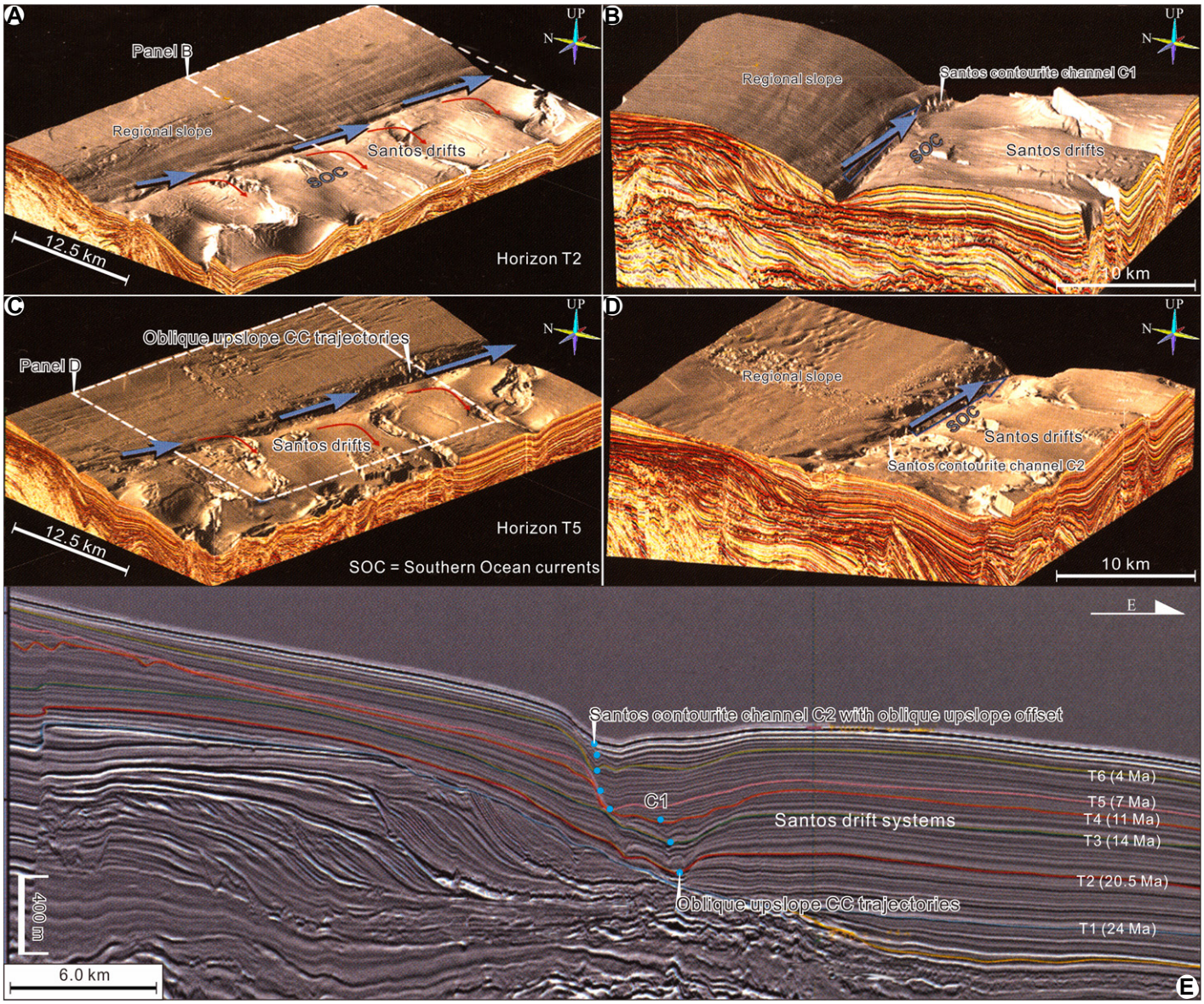

Figure 11. Three-dimensional perspective views of time-structure maps of horizons T2 and T5 (A–D) and depositional dip-view seismic profile (E) (from Duarte and Viana, 2007) showing plan and cross-sectional views of Santos Basin contourite channels (southwestern Atlantic Ocean) with oblique upslope trajectories. Note that upslope channel walls of Santos contourite channels are, overall, steeper than their downslope counterparts. CC—channel complex.

$M_s = 0.59$) and deeper and narrower channel cross-sections (proxied by a lower mean values of $W/T = 17$) (Figs. 15A and 16). The smaller density difference between the contour currents and ambient fluid, in contrast, would increase the potential for overspill and flow stripping. This, in turn, would inhibit channel thalweg deposition (Pirmez and Imran, 2003; Jobe et al., 2016), resulting in more vertical accretion (represented by a lower mean values of $M_s = 0.28$) and shallower but wider channel cross-sections (represented by a higher mean values of $W/T = 39$) (Figs. 15A and 16).

IMPLICATIONS

Approach to a Better Understanding of Channel Stratigraphy between Different Trajectory Regimes

A scatterplot of T_c against M_s for turbidite channels suggests that T_c and M_s follow a power-law relationship (Fig. 8A), expressed as:

$$M_s = 1.6602\ (T_c)^{-0.559}\left(R^2 = 0.62; n = 93\right). \quad (3)$$

Moreover, a cross-plot of T_c versus M_s for contourite channels suggests that T_c and M_s of contourite channels also follow a power-law relationship (Fig. 8B), defined as:

$$M_s = 3\times10^{-9}\left(T_c\right)^{4.13}\left(R^2 = 0.65; n = 46\right). \quad (4)$$

The above two power-law relationships of T_c to M_s for the 142 considered channel examples have a correlation coefficient of $R^2 > 0.60$ and are, thus, solid (Figs. 8A and 8B), suggesting that channel-complex trajectories (proxied by T_c) are predictors of channel stacking styles and

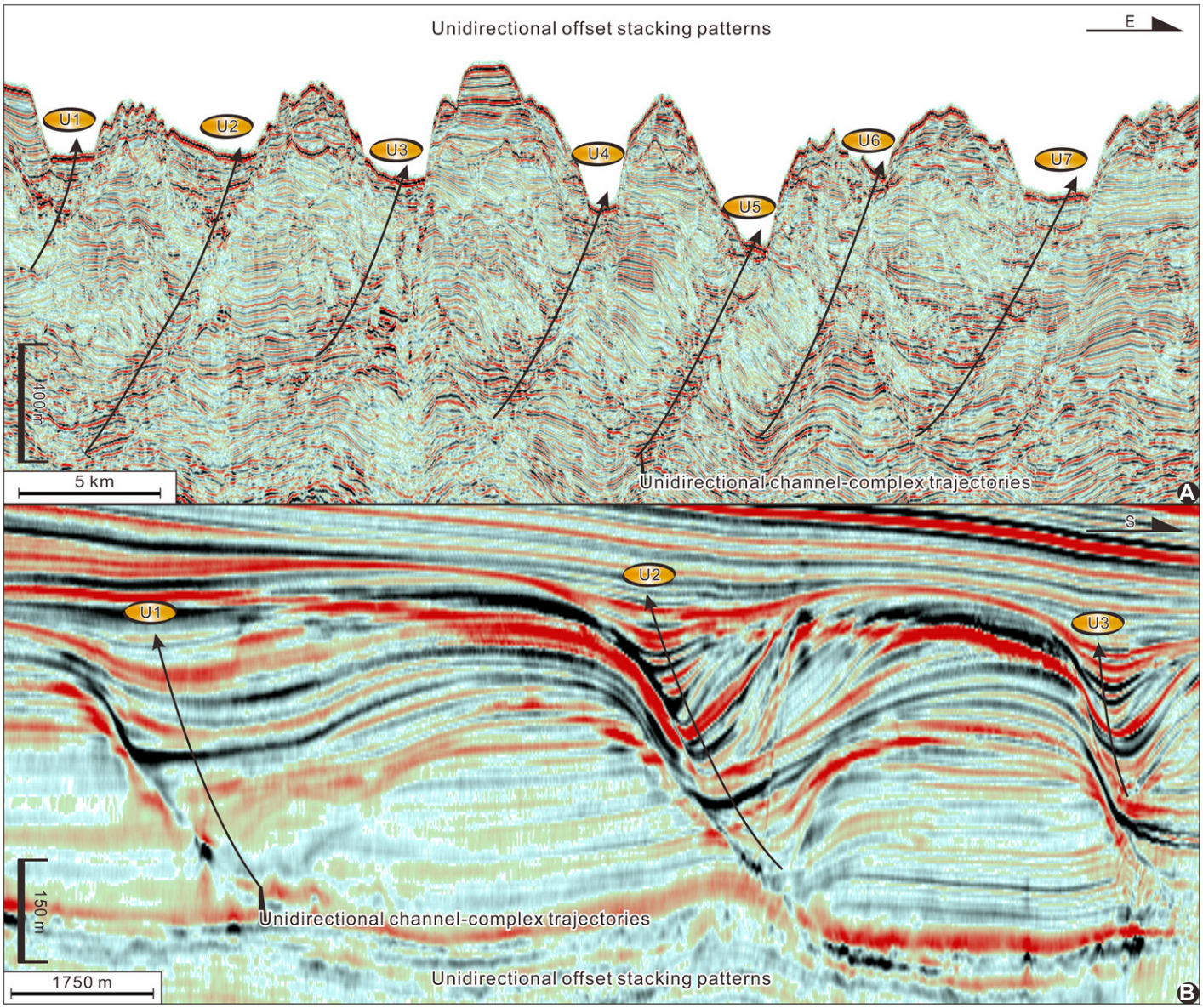

Figure 12. Two-dimensional seismic transect along the depositional dip showing seismic manifestations of unidirectionally migrating deep-water channels in the Pearl River Mouth (northern South China Sea) and Lower Congo Basins (A and B, respectively). The shown channel examples U1 to U7 on panel A and U1 to U3 on panel B are all characterized by unidirectional channel-complex trajectories.

architectures (represented by M_s). Our results, therefore, offer a new approach to interpret submarine channel architectures and stratigraphy, which are ubiquitous on all of Earth's siliciclastic continental margins.

In addition, Jobe et al. (2016) recognized and quantified the hockey-stick trajectory shape of turbidite channels for the first time. However, on the basis of a sampling of 142 submarine channels, two additional types of channel-complex kinematics were recognized (i.e., unidirectional and oblique upslope channel-complex trajectories) in 92 deep-water sites worldwide (numbered white and blue circles in Fig. 1). Unidirectional and oblique upslope channel-complex trajectories are, thus, also fairly common on continental margins worldwide, although they are characterized by channel-complex trajectories that are dramatically different from those of well-documented turbidite channels (e.g., Sylvester et al., 2011; Sylvester and Covault, 2016; Jobe et al., 2016). The present study is the first to quantify their trajectories with a global channel database and to explore autogenic controls on the spatiotemporal evolution of their trajectories, therefore helping to obtain a complete picture of channel kinematics.

Approach to a Better Understanding of Channel Stratigraphy and Population Densities between Different Climate States

Among the 142 chosen channel examples, only 12 cases are grouped into submarine greenhouse channels, with 130 examples categorized as submarine icehouse channels (Tables S1–S3 [footnote 1]; Figs. 1B and 1C). Our results, therefore, suggest that the warmer greenhouse climates were accompanied by the sporadic occurrence of deep-water channels (i.e., 8%), but that the cooler icehouse climates were accompanied by the widespread occurrence of submarine

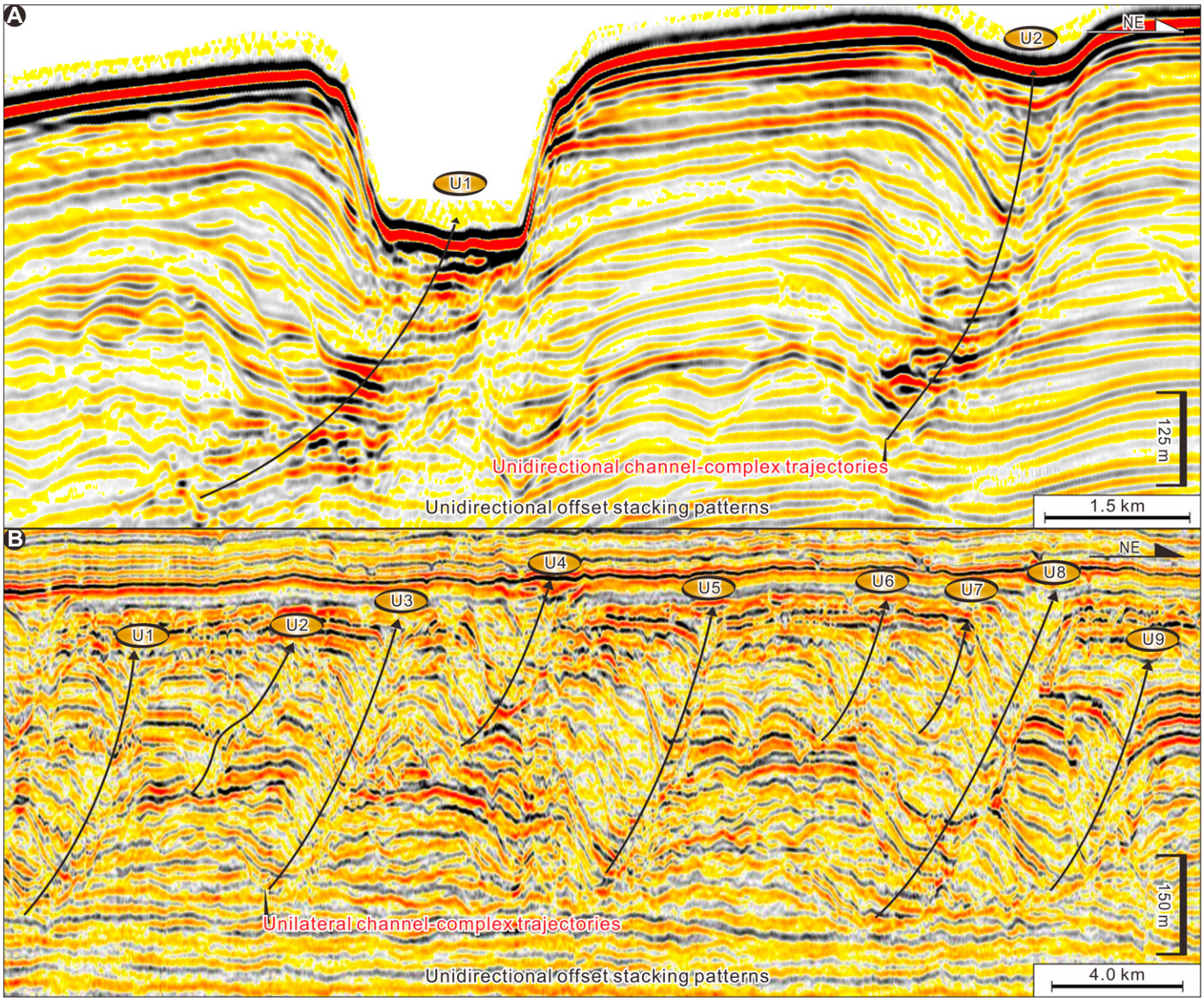

Figure 13. Seismically well-imaged examples of unidirectionally migrating deep-water channels on the western Pearl River slope (U1 to U2 on panel A) and in the eastern Qiongdongnan Basin, northern South China Sea margin (U1 to U9 on panel B).

channels (i.e., 92%), showing an increased channel-population density during cooling icehouse periods versus a decreased channel-population density during warming greenhouse periods (Tables S1–S3 [footnote 1]; Figs. 1B and 1C). Therefore, there has been not a strong global correlation of channel-population density with the global warming. This suggests that future global warming would not make a significant difference to global channel occurrence and probably turbidity current frequencies.

In addition, our results suggest that submarine greenhouse channels are characterized by a low amplitude of morphological and architectural variations, but that submarine icehouse channels are characterized by high amplitudes of morphological and architectural variations (Figs. 15B and 17). Observations and results from the current study, therefore, contribute to a better understanding of how deep-time channel stratigraphy and population densities respond to two end-member types of climatic conditions, which is considered as a key research challenge in the deep-water science community (e.g., Hodgson et al., 2018; Sømme et al., 2019).

CONCLUSIONS

Based on a global sampling of 142 deep-water channels, this study investigates morphologies, architectures, trajectory regimes, and climate states of deep-water channels of different origins, helping to better understand channel stratigraphy.

(1) Five classes of channel-complex trajectories were defined, namely lateral, random, vertical, oblique upslope, and unidirectional channel-complex trajectories. They systematically assemble into three main spatiotemporal evolution styles, including tripartite lateral - random - vertical, oblique upslope, and unidirectional channel-complex trajectories.

(2) Turbidite channels with tripartite lateral - random - vertical or unidirectional channel-complex trajectories have W/T and M_s that are, respectively, two to three times smaller and two to three times larger than those of contourite channels with oblique upslope trajectories,

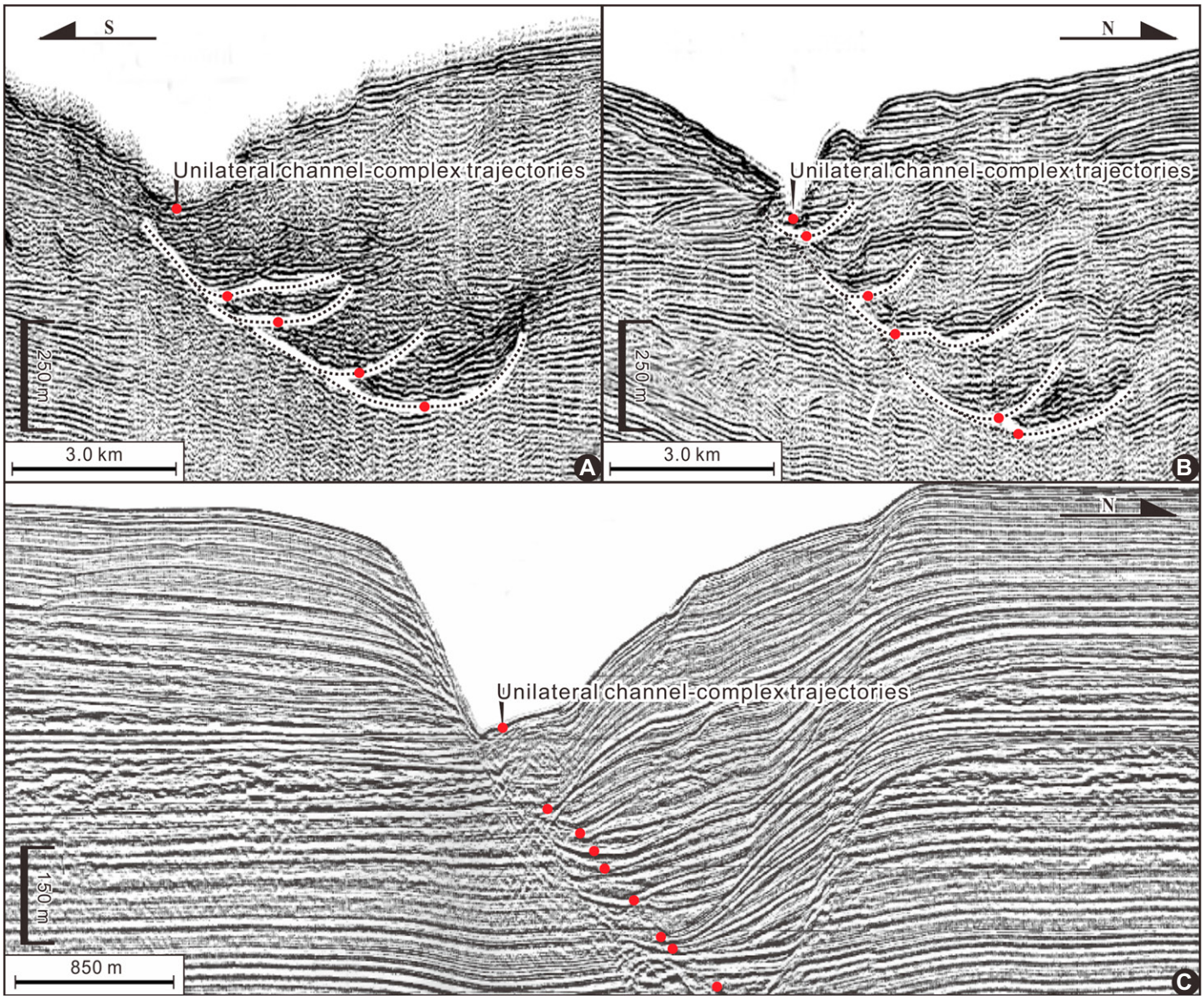

Figure 14. Seismic transects showing typical channel examples with unidirectional channel-complex trajectories on the southeastern Greenland margin (from Rasmussen et al., 2003) (A and B) and the southeastern Brazilian margin (C) (from Faugères et al., 1999).

suggesting that turbidite channels tend to be deep and narrow and have two to three times more lateral migration, but that contourite channels tend to be shallow and wide and have two to three times more vertical accretion. Such differences in channel morphologies and architectures between different trajectory regimes were related to the density contrast in flow and ambient fluid between turbidite versus contourite channels, which would have favored the lateral channel migration in turbidite channels but the vertical channel accretion in contourite channels.

(3) Submarine greenhouse channels display low amplitudes of morphological and architectural variations, whereas icehouse channels exhibit high amplitudes of morphological and architectural variations. Submarine greenhouse and icehouse channels are, respectively, the minority and majority (8% versus 92%) in the global channel family. Such differences in channel-population densities between greenhouse and icehouse channels suggest a weak global correlation of channel-population densities with warming greenhouse climates.

ACKNOWLEDGMENTS

This research was jointly funded by awards from the National Natural Science Foundation of China (41972100), the Major National S and T Program of China (2017ZX05009–002), the Science Foundation of China University of Petroleum, Beijing (2462017YJRC061), and the Independent Project of State Key Laboratory of Petroleum Resources and Prospecting (PRP/indep-1-1701) to C. Gong. Many thanks go to Professor Jingping Xu for taking the time to plough through an early version of this manuscript. We are grateful to GSA Bulletin editors Dr. Rob Strachan and Dr. Rajat Mazumder for editorial handing and comments, and to two anonymous reviewers for their critical and constructive comments, all of which significantly improved the overall quality of this research.

REFERENCES CITED

Azpiroz-Zabala, M., Cartigny, M.J.B., Talling, P.J., Parsons, D.R., Sumner, E.J., Clare, M.A., Simmons, S.M., Cooper, C., and Pope, E.L., 2017, Newly recognized turbidity current structure can explain prolonged flushing of submarine canyons: Science Advances, v. 3, e1700200, https://doi.org/10.1126/sciadv.1700200.

Blum, M.D., and Hattier-Womack, J., 2009, Climatic change, sea-level change, and fluvial sediment supply

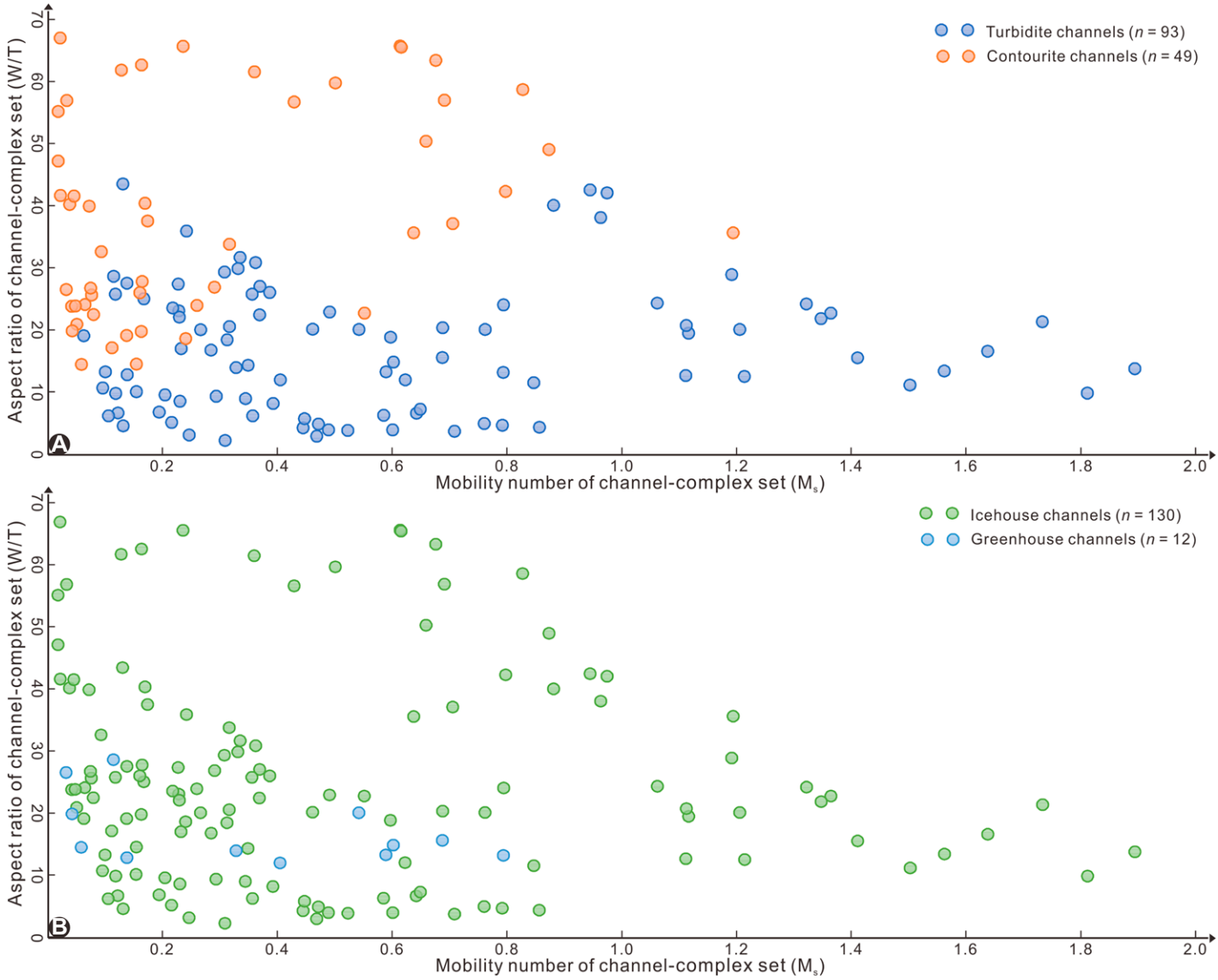

Figure 15. Cross-plots of mobility number (M_s) against the ratio of width to thickness (W/T) for turbidite and contourite channels (A) and for icehouse and greenhouse channels (B).

to deepwater depositional systems, *in* Kneller, B., Martinsen, O.J., McCaffrey, B., eds., External Controls on Deep-Water Depositional Systems: Society of Economic Paleontologists and Mineralogists Special Publication 92, p. 15–39, https://doi.org/10.2110/sepmsp.092.015.

Campbell, D.C., and Mosher, D.C., 2016, Geophysical evidence for widespread Cenozoic bottom current activity from the continental margin of Nova Scotia, Canada: Marine Geology, v. 378, p. 237–260, https://doi.org/10.1016/j.margeo.2015.10.005.

Cossu, R., Wells, M.G., and Peakall, J., 2015, Latitudinal variations in submarine channel sedimentation patterns: The role of Coriolis forces: Journal of the Geological Society, v. 172, p. 161–174, https://doi.org/10.1144/jgs2014-043.

Covault, J.A., Romans, B.W., Fildani, A., McGann, M., and Graham, S.A., 2010, Rapid climatic signal propagation from source to sink in a southern California sediment-routing system: Journal of Geology, v. 118, p. 247–259, https://doi.org/10.1086/651539.

Covault, J.A., Sylvester, Z., Hubbard, S.M., Jobe, Z.R., and Sech, R.P., 2016, The stratigraphic record of submarine-channel evolution: The Sedimentary Record, v. 14, no. 3, p. 4–11, https://doi.org/10.2110/sedred.2016.3.4.

Daly, R.A., 1936, Origin of submarine canyons: American Journal of Science, v. 31, p. 401–420, https://doi.org/10.2475/ajs.s5-31.186.401.

Davies, R., Cartwright, J., Pike, J., and Line, C., 2001, Early Oligocene initiation of North Atlantic Deep Water formation: Nature, v. 410, p. 917–920, https://doi.org/10.1038/35073551.

Deptuck, M.E., Steffens, G.S., Barton, M., and Pirmez, C., 2003, Architecture and evolution of upper fan channel-belts on the Niger Delta slope and in the Arabian Sea: Marine and Petroleum Geology, v. 20, p. 649–676, https://doi.org/10.1016/j.marpetgeo.2003.01.004.

Duarte, C.S.L., and Viana, A.R., 2007. Santos Drift System: Stratigraphic organization and implications for late Cenozoic palaeocirculation in the Santos Basin, SW Atlantic Ocean, *in* Viana, A.R., and Rebesco, M., eds., Economic and Palaeoceanographic Significance of Contourite Deposits: Geological Society of London Special Publication 276, p. 171–198, https://doi.org/10.1144/GSL.SP.2007.276.01.09.

Edwards, C., McQuaid, S., Easton, S., Scott, D., Couch, A., Evans, R., and Hart, S., 2017. Lateral accretion in a straight slope channel system: An example from the Forties Sandstone of the Huntington Field, UK Central North Sea, *in* Bowman, M., and Levell, B., eds., Petroleum Geology of NW Europe: 50 Years of Learning—Proceedings of the 8th Petroleum Geology Conference: Geological Society of London Petroleum Geology Conference Series 8, p. 413–428, https://doi.org/10.1144/PGC8.33.

Faugères, J.-C., Stow, D.A.V., Imbert, P., and Viana, A., 1999, Seismic features diagnostic of contourite drifts: Marine Geology, v. 162, p. 1–38, https://doi.org/10.1016/S0025-3227(99)00068-7.

Fildani, A., 2017, Submarine Canyons: A brief review looking forward: Geology, v. 45, p. 383–384, https://doi.org/10.1130/focus042017.1.

Fonnesu, M., Palermo, D., Galbiati, M., Marchesini, M., Bonamini, E., and Bendias, D., 2020, A new world-class deep-water play-type, deposited by the syndepositional interaction of turbidity flows and bottom currents: The giant Eocene Coral Field in northern Mozambique: Marine and Petroleum

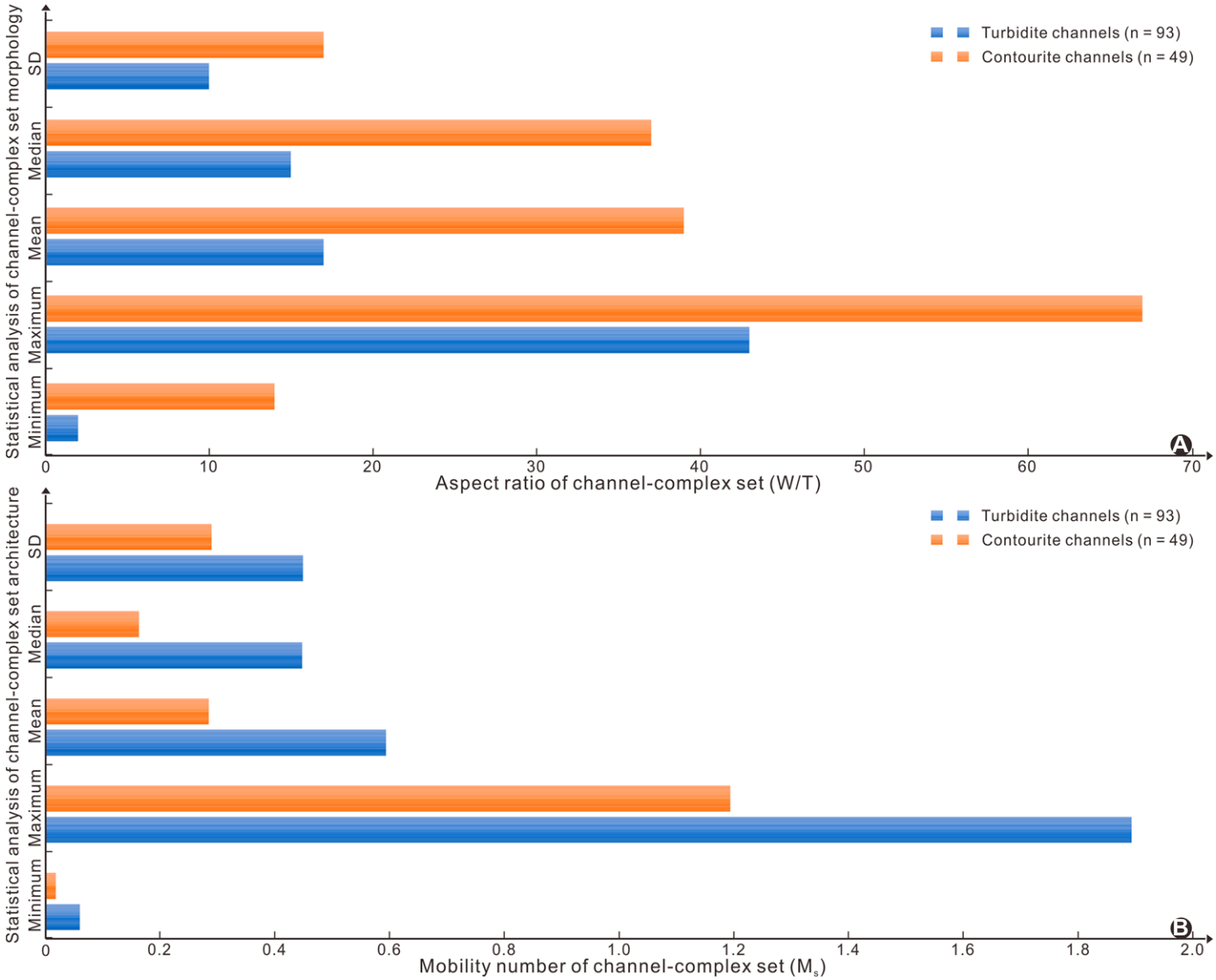

Figure 16. Statistical analyses of ratio of width to thickness (*W*/*T*) (A) and mobility number (M_s) (B) of turbidite versus contourite channels (SD—standard deviation).

Geology, v. 111, p. 179–201, https://doi.org/10.1016/j.marpetgeo.2019.07.047.

Fournier, L., Fauquembergue, K., Zaragosi, S., Zorzi, C., Malaizé, B., Bassinot, F., Joussain, R., Colin, C., Moreno, E., and Leparmentier, F., 2016, The Bengal fan: External controls on the Holocene Active Channel turbidite activity: The Holocene, v. 27, p. 900–913, https://doi.org/10.1177/0959683616675938.

Galy, V., France-Lanord, C., Beyssac, O., Faure, P., Kudrass, H., and Palhol, F., 2007, Efficient organic carbon burial in the Bengal fan sustained by the Himalayan erosional system: Nature, v. 450, p. 407–410, https://doi.org/10.1038/nature06273.

Gong, C., Wang, Y., Zhu, W., Li, W., and Xu, Q., 2013, Upper Miocene to Quaternary unidirectionally migrating deep-water channels in the Pearl River Mouth Basin, northern South China Sea: American Association of Petroleum Geologists Bulletin, v. 97, p. 285–308, https://doi.org/10.1306/07121211159.

Gong, C., Peakall, J., Wang, Y., Wells, M.G., and Xu, J., 2017, Flow processes and sedimentation in contourite channels on the northwestern South China Sea margin: A joint 3D seismic and oceanographic perspective: Marine Geology, v. 393, p. 176–193, https://doi.org/10.1016/j.margeo.2016.11.002.

Gong, C., Wang, Y., Rebesco, M., Salon, S., and Steel, R.J., 2018, How do turbidity flows interact with contour currents in unidirectionally migrating deep-water channels?: Geology, v. 46, p. 551–554, https://doi.org/10.1130/G40204.1.

Henrich, R., Cherubini, Y., and Meggers, H., 2010, Climate and sea level induced turbidite activity in a canyon system offshore the hyperarid Western Sahara (Mauritania): The Timiris Canyon: Marine Geology, v. 275, p. 178–198, https://doi.org/10.1016/j.margeo.2010.05.011.

Hodgson, D.M., Bernhardt, A., Clare, M.A., Da Silva, A.-C., Fosdick, J.C., Mauz, B., Midtkandal, I., Owen, A., and Romans, B.W., 2018, Grand challenges (and great opportunities) in sedimentology, stratigraphy, and diagenesis research: Frontiers of Earth Science, v. 6, 173, https://doi.org/10.3389/feart.2018.00173.

Hohbein, M., and Cartwright, J., 2006, 3D seismic analysis of the West Shetland Drift system: Implications for Late Neogene palaeoceanography of the NE Atlantic: Marine Geology, v. 230, p. 1–20, https://doi.org/10.1016/j.margeo.2006.03.009.

Hubbard, S.M., Covault, J.A., Fildani, A., and Romans, B.W., 2014, Sediment transfer and deposition in slope channels: Deciphering the record of enigmatic deep-sea processes from outcrop: Geological Society of America Bulletin, v. 126, p. 857–871, https://doi.org/10.1130/B30996.1.

Janocko, M., Nemec, W., Henriksen, S., and Warchoł, M., 2013, The diversity of deep-water sinuous channel belts and slope valley-fill complexes: Marine and Petroleum Geology, v. 41, p. 7–34, https://doi.org/10.1016/j.marpetgeo.2012.06.012.

Jerolmack, D.J., and Mohrig, D., 2007, Conditions for branching in depositional rivers: Geology, v. 35, p. 463–466, https://doi.org/10.1130/G23308A.1.

Jobe, Z.R., Sylvester, Z., Parker, A.O., Howes, N., Slowey, N., and Pirmez, C., 2015, Rapid adjustment of submarine channel architecture to changes in sediment supply: Journal of Sedimentary Research, v. 85, p. 729–753, https://doi.org/10.2110/jsr.2015.30.

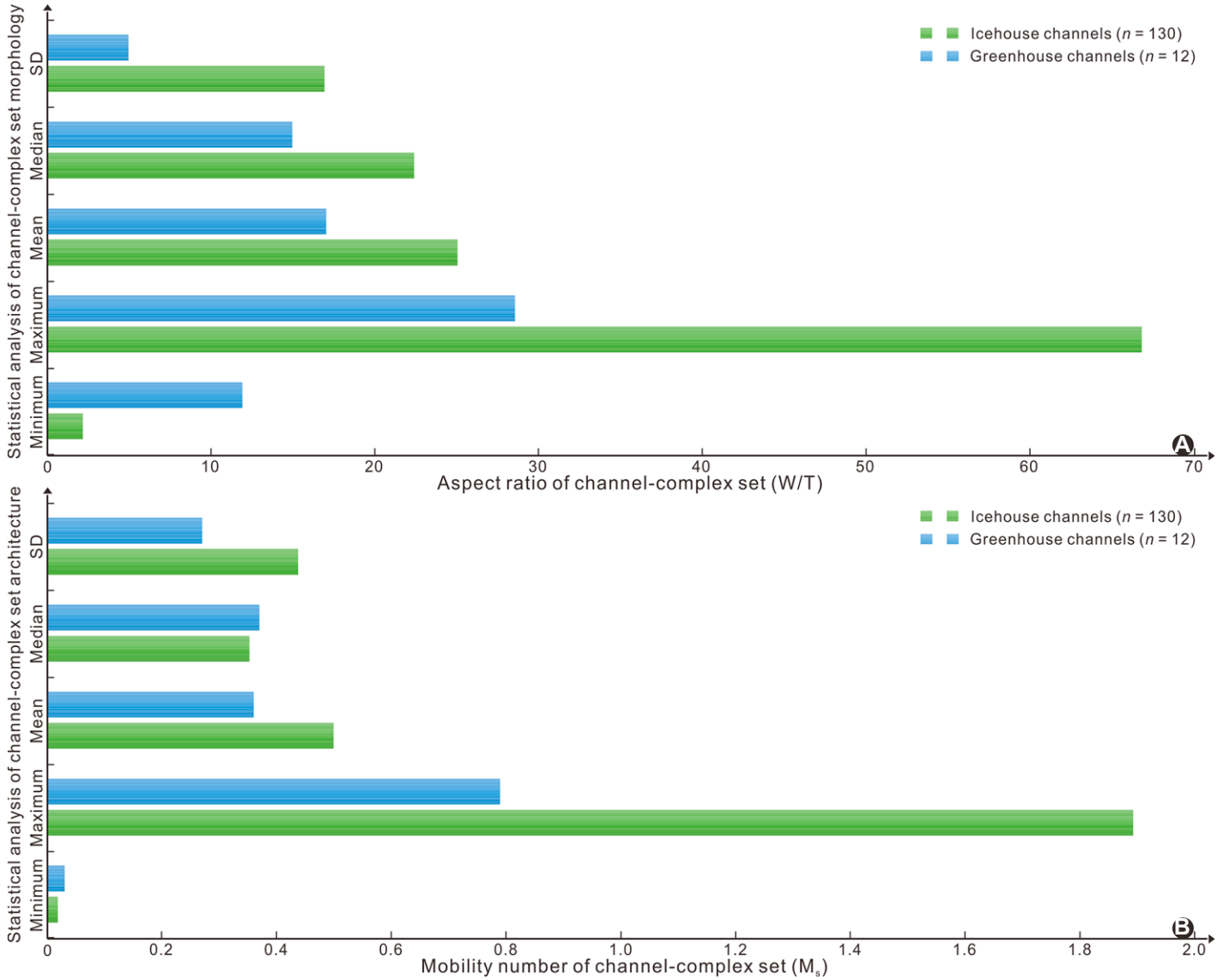

Figure 17. Statistical analyses of ratio of width to thickness (*W/T*) (A) and mobility number (M_s) (B) of icehouse versus greenhouse channels (SD—standard deviation).

Jobe, Z.R., Howes, N.C., and Auchter, N.C., 2016, Comparing submarine and fluvial channel kinematics: Implications for stratigraphic architecture: Geology, v. 44, p. 931–934, https://doi.org/10.1130/G38158.1.

Kidder, D.L., and Worsley, T.R., 2012, A human-induced hothouse climate?: GSA Today, v. 22, no. 2, p. 4–11, https://doi.org/10.1130/G131A.1.

Kolla, V., Posamentier, H.W., and Wood, L.J., 2007, Deep-water and fluvial sinuous channels: Characteristics, similarities and dissimilarities, and modes of formation: Marine and Petroleum Geology, v. 24, p. 388–405, https://doi.org/10.1016/j.marpetgeo.2007.01.007.

Labourdette, R., and Bez, M., 2009, Element migration in turbidite systems: Random or systematic depositional processes?: American Association of Petroleum Geologists Bulletin, v. 94, p. 345–368, https://doi.org/10.1306/09010909035.

Lu, H., Fulthorpe, C.S., and Mann, P., 2003, Three-dimensional architecture of shelf-building sediment drifts in the offshore Canterbury Basin, New Zealand: Marine Geology, v. 193, p. 19–47, https://doi.org/10.1016/S0025-3227(02)00612-6.

Mayall, M., Jones, E., and Casey, M., 2006, Turbidite channel reservoirs—Key elements in facies prediction and effective development: Marine and Petroleum Geology, v. 23, p. 821–841, https://doi.org/10.1016/j.marpetgeo.2006.08.001.

McHargue, T., Pyrcz, M.J., Sullivan, M.D., Clark, J.D., Fildani, A., Romans, B.W., Covault, J.A., Levy, M., Posamentier, H.W., and Drinkwater, N.J., 2011, Architecture of turbidite channel systems on the continental slope: Patterns and predictions: Marine and Petroleum Geology, v. 28, p. 728–743, https://doi.org/10.1016/j.marpetgeo.2010.07.008.

Miller, K.G., Wright, J.D., and Fairbanks, R.G., 1991, Unlocking the Ice House: Oligocene-Miocene oxygen isotopes, eustasy, and margin erosion: Journal of Geophysical Research, v. 96, p. 6829–6848, https://doi.org/10.1029/90JB02015.

Miller, K.G., Sugarman, P.J., Browning, J.V., Kominz, M.A., Hernández, J.C., Olsson, R.K., Wright, J.D., Feigenson, M.D., and Sickel, W.V., 2003, Late Cretaceous chronology of large, rapid sea-level changes: Glacioeustasy during the greenhouse world: Geology, v. 31, p. 585–588, https://doi.org/10.1130/0091-7613(2003)031<0585:LCCOLR>2.0.CO;2.

Miramontes, E., Eggenhuisen, J.T., Jacinto, R.S., Poneti, G., Pohl, F., Normandeau, A., Campbell, D.C., and Hernández-Molina, F.J., 2020, Channel-levee evolution in combined contour current–turbidity current flows from flume-tank experiments: Geology, v. 48, p. 353–357, https://doi.org/10.1130/G47111.1.

Peakall, J., and Sumner, E.J., 2015, Submarine channel flow processes and deposits: A process-product perspective: Geomorphology, v. 244, p. 95–120, https://doi.org/10.1016/j.geomorph.2015.03.005.

Peakall, J., McCaffrey, W.D., and Kneller, B.C., 2000, A process model for the evolution, morphology, and architecture of sinuous submarine channels: Journal of Sedimentary Research, v. 70, p. 434–448, https://doi.org/10.1306/2DC4091C-0E47-11D7-8643000102C1865D.

Pirmez, C., and Imran, J., 2003, Reconstruction of turbidity currents in Amazon Channel: Marine and Petroleum Geology, v. 20, p. 823–849, https://doi.org/10.1016/j.marpetgeo.2003.03.005.

Posamentier, H.W., 2003, Depositional elements associated with a basin floor channel-levee system: case study from the Gulf of Mexico: Marine and Petroleum Geology, v. 20, p. 677–690, https://doi.org/10.1016/j.marpetgeo.2003.01.002.

Puig, P., Ogston, A.S., Mullenbach, B.L., Nittrouer, C.A., Parsons, J.D., and Sternberg, R.W., 2004, Storm-induced sediment gravity flows at the head of the Eel submarine canyon, northern California margin: Journal of Geophysical Research, v. 109, C03019, https://doi.org/10.1029/2003JC001918.

Rasmussen, S., Lykke-Andersen, H., Kuijpers, A., and Troelstra, S.R., 2003, Post-Miocene sedimentation at the continental rise of Southeast Greenland: The interplay between turbidity and contour currents: Marine Geology, v. 196, p. 37–52, https://doi.org/10.1016/S0025-3227(03)00043-4.

Rebesco, M., Hernández-Molina, F.J., Van Rooij, D., and Wåhlin, A., 2014, Contourites and associated sediments controlled by deep-water circulation processes: State-of-the-art and future considerations: Marine Geology, v. 352, p. 111–154, https://doi.org/10.1016/j.margeo.2014.03.011.

Sansom, P., 2018, Hybrid turbidite-contourite systems of the Tanzanian margin: Petroleum Geoscience, v. 24, p. 258–276, https://doi.org/10.1144/petgeo2018-044.

Sequeiros, O.E., Pittaluga, M.B., Frascati, A., Pirmez, C., Masson, D.G., Weaver, P., Crosby, A.R., Lazzaro, G., Botter, G., and Rimmer, J.G., 2019, How typhoons trigger turbidity currents in submarine canyons: Scientific Reports, v. 9, 9220, https://doi.org/10.1038/s41598-019-45615-z.

Séranne, M., and Abeigne, C.-R.N., 1999, Oligocene to Holocene sediment drifts and bottom currents on the slope of Gabon continental margin (West Africa): Consequences for sedimentation and southeast Atlantic upwelling: Sedimentary Geology, v. 128, p. 179–199, https://doi.org/10.1016/S0037-0738(99)00069-X.

Shepard, F.P., and Emery, K.O., 1941, Submarine Topography off the California Coast: Canyons and Tectonic Interpretations: Geological Society of America Special Paper 31, 171 p.

Sømme, T.O., Helland-Hansen, W., and Granjeon, D., 2009, Impact of eustatic amplitude variations on shelf morphology, sediment dispersal, and sequence stratigraphic interpretation: Icehouse versus greenhouse systems: Geology, v. 37, p. 587–590, https://doi.org/10.1130/G25511A.1.

Sømme, T.O., Skogseid, J., Embry, P., and Løseth, H., 2019, Manifestation of tectonic and climatic perturbations in deep-time stratigraphy—An example from the Paleocene succession offshore western Norway: Frontiers of Earth Science, v. 7, 303, https://doi.org/10.3389/feart.2019.00303.

Sprague, A.R., Sullivan, M.D., Campion, K.M., Jensen, G.N., Goulding, F.J., Garfield, T.R., Sickafoose, D.K., Rossen, C., Jennette, D.C., Beaubouef, R.T., Abreu, V., Ardill, J., Porter, M.L., and Zelt, F.B., 2002, The physical stratigraphy of deep-water strata: A hierarchical approach to the analysis of genetically related stratigraphic elements for improved reservoir prediction: Abstract presented at American Association of Petroleum Geologists Annual Meeting, Houston, Texas, 10–13 March.

Stoll, H.M., and Schrag, D.P., 1996, Evidence for glacial control of rapid sea level changes in the early Cretaceous: Science, v. 272, p. 1771–1774, https://doi.org/10.1126/science.272.5269.1771.

Sumner, E.J., Peakall, J., Dorrell, R.M., Parsons, D.R., Darby, S.E., Wynn, R.B., McPhail, S.D., Perrett, J., Webb, A., and White, D., 2014, Driven around the bend: Spatial evolution and controls on the orientation of helical bend flow in a natural submarine gravity current: Journal of Geophysical Research: Oceans, v. 119, p. 898–913, https://doi.org/10.1002/2013JC009008.

Surlyk, F., Jensen, S.K., and Engkilde, M., 2008, Deep channels in the Cenomanian–Danian Chalk Group of the German North Sea sector: Evidence of strong constructional and erosional bottom currents and effect on reservoir quality distribution: American Association of Petroleum Geologists Bulletin, v. 92, p. 1565–1586, https://doi.org/10.1306/07100808035.

Sylvester, Z., and Covault, J.A., 2016, Development of cut-off-related knickpoints during early evolution of submarine channels: Geology, v. 44, p. 835–838, https://doi.org/10.1130/G38397.1.

Sylvester, Z., Pirmez, C., and Cantelli, A., 2011, A model of submarine channel-levee evolution based on channel-growth trajectories: Implications for stratigraphic architecture: Marine and Petroleum Geology, v. 28, p. 716–727, https://doi.org/10.1016/j.marpetgeo.2010.05.012.

Symons, W.O., Sumner, E.J., Paull, C.K., Cartigny, M.J.B., Xu, J.P., Maier, K.L., Lorenson, T.D., and Talling, P.J., 2017, A new model for turbidity current behavior based on integration of flow monitoring and precision coring in a submarine canyon: Geology, v. 45, p. 367–370, https://doi.org/10.1130/G38764.1.

Talling, P.J., Wynn, R.B., Masson, D.G., Frenz, M., Cronin, B.T., Schiebel, R., Akhmetzhanov, A.M., Dallmeier-Tiessen, S., Benetti, S., Weaver, P.P.E., Georgiopoulou, A., Zühlsdorff, C., and Amy, L.A., 2007, Onset of submarine debris flow deposition far from original giant landslide: Nature, v. 450, p. 541–544, https://doi.org/10.1038/nature06313.

Wynn, R.B., Cronin, B.T., and Peakall, J., 2007, Sinuous deep-water channels: Genesis, geometry and architecture: Marine and Petroleum Geology, v. 24, p. 341–387, https://doi.org/10.1016/j.marpetgeo.2007.06.001.

Zhang, Y., Liu, Z., Zhao, Y., Colin, C., Zhang, X., Wang, M., Zhao, S., and Kneller, B., 2018, Long-term *in situ* observations on typhoon-triggered turbidity currents in the deep sea: Geology, v. 46, p. 675–678, https://doi.org/10.1130/G45178.1.

Science Editor: Rob Strachan
Associate Editor: Rajat Mazumder

Manuscript Received 16 July 2019
Revised Manuscript Received 27 March 2020
Manuscript Accepted 16 April 2020

Printed in the USA